Design of the Dullomatic: a Mechanical Follow-the-Leader Device

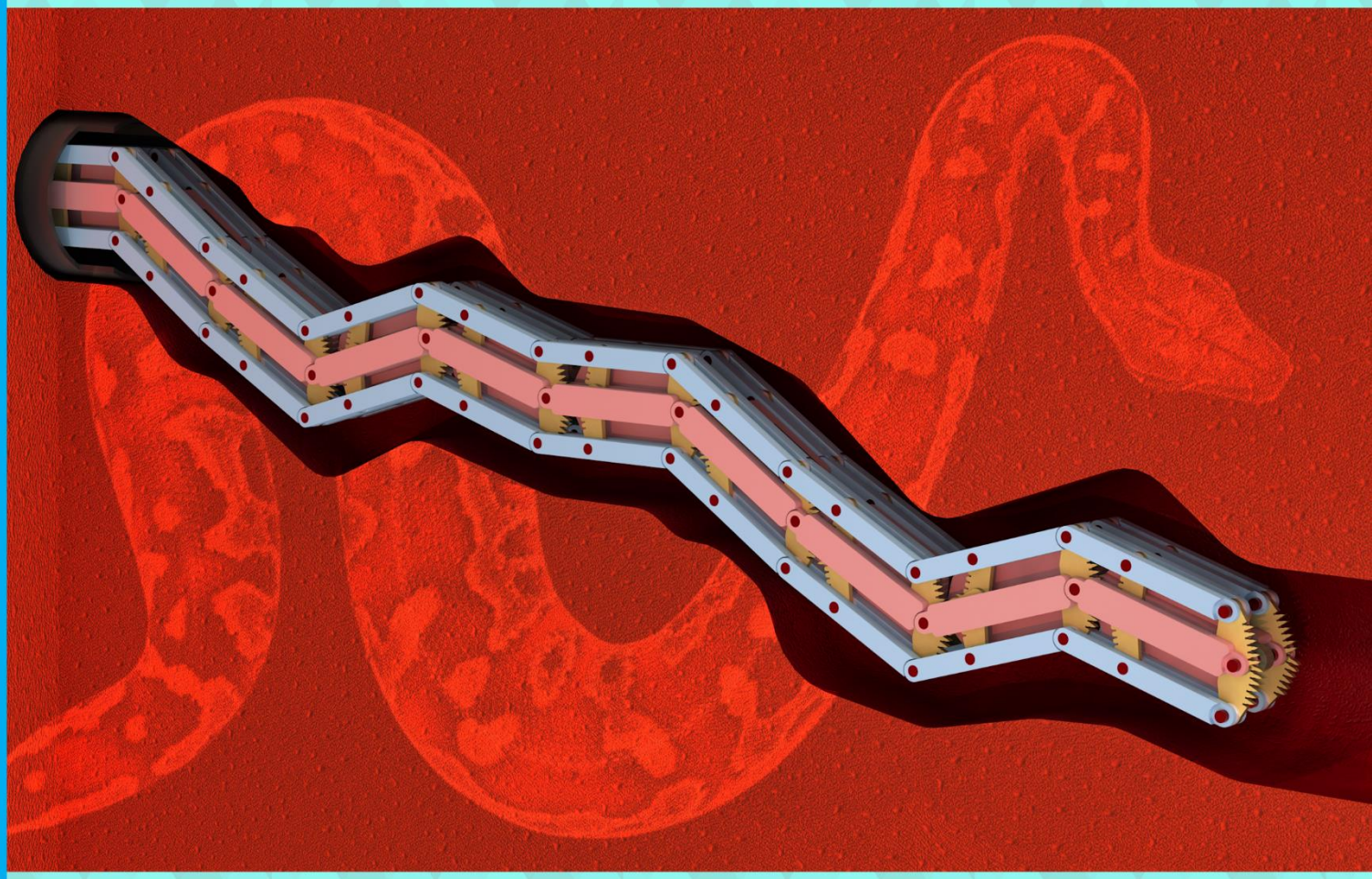

Daan Dullaart

TU Delft

Design of the Dullomatic: a Mechanical Follow-the-Leader Device

By

Daan Dullaart

in partial fulfilment of the requirements for the degree of

Master of Science

in Mechanical Engineering

at the Delft University of Technology,

to be defended publicly on Friday May 26, 2023 at 2:00 PM.

Student Number:	4170903
Supervisors:	Prof. dr. ir. P. Breedveld
	MSc. ir. K. Lussenburg
	MSc ir. F. Trauzettel
Thesis committee:	Prof. dr. ir. P. Breedveld, TU Delft
	Dr. ir. T. Horeman, TU Delft

TU Delft

Preface

From an early age I have been fascinated by technology and nature, and the two came together in the master course Bio-Inspired Design, lectured by Paul Breedveld. Delving into nature's ingenious solutions to gather inspiration for solving complex engineering problems is intriguing. I therefore wanted to complete my master thesis in the bio-inspired-technology group (BITE) at the TU Delft. While searching for an assignment, I came across a graduation assignment regarding hierarchical mechanisms. This assignment explored building large mechanisms using small mechanism as building blocks. Since the assignment specifically mentioned that they were looking for a creative student with a curious mind, I knew the project was right up my alley. I contacted the supervisor Kirsten Lussenburg, and shortly after I was able to start this graduation trajectory.

After writing a literature review on bio-inspired 3D-printed designs, I started exploring hierarchical mechanisms. This topic is extensive, hence it was difficult to choose a specific mechanism or application. Paul Breedveld suggested to design one particular hierarchical mechanism: a follow-the-leader device. Seeing how mechanically complex these devices are, I accepted the challenge. Designing the mechanism was a challenging and enjoyable process, with a result beyond my own expectations.

I want to thank Paul Breedveld for his advice, insight and stimulating meetings that provided plenty of food for thought. I also want to thank Kirsten Lussenburg for her expertise, patience and guidance throughout the project. I want to thank Fabian Trauzettel for his knowledge, revisions on my thesis and the fun chats. I want to thank David Jager and Remi van Starkenburg from DEMO for assisting in the realization of the prototype and the manufacturing of its parts. I want to thank my parents, sister, and friends for supporting me throughout my studies. Lastly, I want to express my gratitude to all those who protect and preserve nature, for it is invaluable and irreplaceable.

Daan Dullaart, 25-03-2023

Abstract

Minimally invasive surgery (MIS) has several advantages over conventional surgery, including reduced damage to the body, less pain, lower infection risk, and faster recovery. However, MIS reduces the amount of space in which clinicians can operate within the body. This often forces them to work around delicate anatomical structures. A new type of instrument that can manoeuvre the body with snake-like movement, also called follow-the-leader (FTL) locomotion, could be a solution. A challenging design aspect of FTL instruments is to conserve the instrument's shape accurately while the instrument propagates into or retracts from the body. This thesis presents a new device, called the Dullomatic, which can conserve 2D shapes and fits inside an instrument's flexible shaft. The Dullomatic contains two adjacent mechanical shape memories which alternate between a flexible and rigid state, together forming a shaft. The device can be operated such that it conserves the shape and shifts the shape backwards as the device propagates forwards, or vice versa, to attain FTL locomotion. A prototype of this design was manufactured at a 2:1 scale containing 3 segments per shape memory. This prototype was evaluated by performing four FTL steps over a curved trajectory and measuring the position of the segments after each step. The results show that the device could be operated to accurately follow this path with FTL locomotion. Further research is required to enhance its user interface and investigate its potential for miniaturization. The Dullomatic forms an interesting addition in the field of FTL devices and might be able to aid in further reducing the invasiveness of surgery.

Contents

1 Introduction

1.1 Background minimally invasive surgery

In conventional open surgery, skin and tissue are cut open to give the surgeon a view of the underlying tissues and organs while offering a large entry point for surgical instruments. A different method is minimally invasive surgery (MIS), in which only a small incision is made allowing slender tools to reach the target. This has the benefit of causing less damage to the body, resulting in less pain, a lower chance of infection and a faster recovery of the patient [1].

One of the first MIS procedures is laparoscopy, in which the internal organs in the abdominal cavity and pelvic area can be inspected and operated on [2]. An incision in the abdominal region is made to allow a thin rigid tube containing a camera and light (a laparoscope) to enter the abdominal cavity, allowing the surgeon to inspect the internal organs. An additional incision is required for each extra instrument. It is preferred to create only a single small incision and have a multifunctional instrument pass through it, as this further minimizes the damage to the body [3]. In some cases an anatomic orifice can be used to reach the target. The nose can be used to reach some anterior areas of the brain in endoscopic endonasal surgery [4], whereas the mouth, anus, vagina and urethra can be used to access areas in the abdomen in natural orifice transluminal endoscopic surgery (NOTES)[5].

For the MIS instrument to fit through natural orifices, its outer diameter should not exceed the diameter of the natural orifice. The maximum shaft diameter depends both on the access point and path, which is operation specific. For example, the nostrils have a diameter of 10 mm [6], and the diameter of colonoscopes fall between 10 mm and 12 mm [7]. Even smaller are the common femoral artery at 6.6 mm [8] and the radial artery at 2.3 mm [9], which are used in cardiac catheterization. The dimensions of these natural orifices also varies between patients.

The pathway between the access point and the target area can be obstructed by anatomical structures. In some cases an anatomical pathway does exist but has various curves, like the colon. Rigid instruments cannot be used in these situations, but flexible instruments can be used as they can follow the complex anatomical pathways. Passively flexible instruments, such as catheters, can be used when an anatomical pathway is present and provides support and guidance to the instrument. However, when there is no anatomical pathway, or the anatomical pathway cannot provide support due to the flexibility or vulnerability of the tissue, an instrument with actively controlled flexibility is required.

Actively controlled flexibility is found in a range of instruments that can transition between a flexible and rigid state [10]. These instruments navigate the body in a flexible state and turn rigid when the instrument needs to apply force. When the instrument is completely flexible during navigation, it has the same downside as passively flexible instruments, as it still requires support from the anatomical pathway. A branch of actively controlled flexible instruments exists in which the instrument is rigid enough to not require support, while remaining steerable. The shape of these instrument is controlled using a control method called follow-the-leader (FTL).

FTL control is inspired by serpentine locomotion, and was first used in hyper-redundant robots [11]. FTL locomotion is illustrated in Figure 1. In this type of locomotion, the path is determined by the so-called leader (the snake's head), while the rest (the snake's body) follows the path that has been set out. This way, a snake, or a snake-like instrument, can move past obstacles without the body colliding with the obstacles during forward (or backward) locomotion [12].

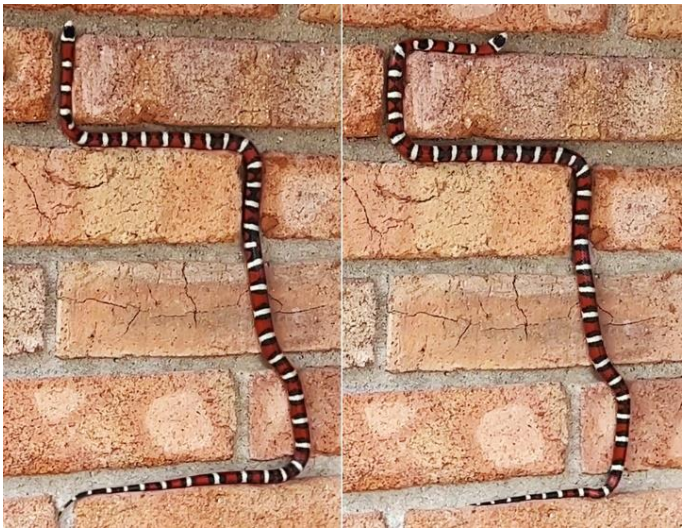

Figure 1: Follow the leader locomotion of a Sonoran mountain kingsnake on a brick wall. The snake can navigate past obstacles by steering its head around the obstacle, while their body follows the created path. Adapted from [13].

MIS instruments with FTL locomotion offer several large benefits. First of all, these instruments can move through complex pathways, which broadens the range of possible access points. Either a natural orifice can be used, or the incision can be made at a location that is more beneficial for the patient in terms of recovery, pain, and/or formation of scar tissue. Hence, the invasiveness of the surgical procedure is reduced [14]. Secondly, these instruments can be steered past delicate tissue without applying force on that tissue, avoiding pain and damage. The instrument can also advance forward or be retracted without colliding with any of the tissues it has circumvented. Thirdly, the manoeuvrability of the

instrument increases the access to the diseased area, as the end-effector can be steered to reach the target from different angles.

1.2 State of the art FTL medical devices

Functions of FTL medical devices

A literature review on FTL locomotion in medical devices has been carried out by Culmone *et al.* [15]. They identified three sub-functions of FTL systems and categorized their literature search results based on them. These sub-functions are:

- Steering
- Propagation along the path towards the target
- Conservation of shape

These sub-functions are illustrated in Figure 2, and are described using the snake as an example. Steering occurs at the head, which has several degrees of freedom and can use its sensors to find the best path around an obstacle. Propagation is the forward (or backwards) motion of the snake. Conservation of shape is attained in the rest of the body through the cooperation between the musculoskeletal system and nervous system.

Figure 2: Functions of an FTL instrument graphically displayed using a snake as an example. The head of the snake steers, while the body conserves the shape. The forward motion of the shape is called propagation. Adapted from [13].

Structure

A schematic representation of a FTL MIS instrument is displayed in Figure 3, showing the structure and the key components these instruments are likely to contain. These components are:

- A segmented shaft containing:
  - A leader segment
  - Multiple follower segments
- A control module
- A transmission
- A track

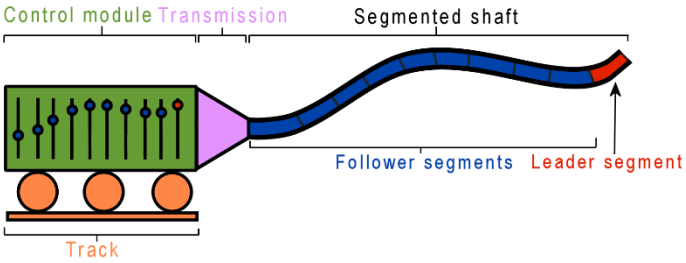

Figure 3: Schematic representation of a FTL MIS instrument, based on the designs of the MemoFlex and MemoFlex II [16][17]*. The instrument consists of a control module, transmission, and segmented shaft. The shaft consists of a leader segment and follower segments. The instrument is placed on a track for accurate propagation.*

The segmented shaft is the only part of the instrument that enters the body during surgery, while the control module and transmission stay outside. The shaft consists of segments, which discretizes the shape. The segment at the tip of the instrument is called the leader, whereas the rest of the shaft consists of follower segments. The instrument can be mounted entirely or partly on a track.

The leader segment's function is steering, and it can contain a small camera for visual assistance. The leader segment can also contain a surgical tool such as a scissor or a forceps. The follower segment's function is to conserve the shape. The shape of the shaft is discretized in the shaft segments, hence the number of segments and the length of each segment determines the number of shapes the instrument can obtain. The control module controls the degree of freedom (DOF) of each individual shaft segment. The control module and the segmented shaft are connected through a transmission, which passes the outputs of the control module to the shaft segments. For example, if the instrument is a mechatronic system, the transmission consists of wires connecting the control module (a computer) to actuators in each segment of the shaft. The instrument is mounted on a track to control the forward and backwards motion of the instrument.

Design challenges

Conservation of shape poses the biggest challenge in the design of an FTL instrument. The follower segments together have a large number of DOF that must be controlled accurately to obtain FTL locomotion. A micro-actuator can be used to control a single DOF accurately, but they are too large to fit inside the follower segments. Furthermore, actuators for medical instruments are expensive, and a large number of them would be required to control the DOF of all follower segments. Therefore, many state-of-the-art designs focus on mechanical solutions for conservation of shape. Different

mechanisms have been designed to conserve the shape, and they are either integrated in the shaft, or placed outside the shaft.

Conserving the shape through a mechanism inside the shaft is achieved by so called alternating devices. These devices consist of two shafts which alternate between a flexible and rigid state [18][19][20][21][22]. When one shaft is rigid, it conserves the shape and functions as physical guidance to the flexible shaft that can slide along it. The flexible shaft can advance forward and be steered into a new direction before it is turned rigid. This cycle is repeated during propagation. To turn a shaft from flexible to rigid, alternating devices use mechanisms relying on friction [19][20][21] or geometrical shape locks [18]. Friction is not reliable, as small amounts of slip will cause the shape to be gradually lost over time. Geometrical shape locks are more reliable but have led to a complicated shaft design that is difficult to miniaturize.

Several designs control the DOF of the follower segments from a control module positioned outside the shaft [16][17][23][24], similar to the illustration in Figure 3. The control module can be much larger than the shaft as it stays outside the body, which relaxes its dimensional requirements. The shaft itself does not have to contain this mechanism and can therefore be miniaturized more conveniently. Mechanical FTL control modules can conserve the shape accurately and provide the required FTL control [24]. They are also referred to as mechanical shape memories, as they memorize the shape of the instrument. These designs inherently require a transmission that connects the control module to the follower segments. Current transmissions consist of cables placed under tension, forming a physical connection between the control module and each of the follower segments. The cables stretch under the tension required to control the follower segments, which dampens the shape of the shaft [17].

Steering the leader segment is an easier task, as only two DOF have to be controlled. A transmission can be used to connect the leader segment to a control module outside the shaft. Any error inside the transmission can be compensated for directly, as the surgeon can continue to give steering input until the leader segment has the correct orientation. Therefore, errors in the transmission are not as detrimental to steering as they are to conserving the shape.

Lastly, propagation is relatively simple, because the instrument can be placed on a track positioned outside the body. It can therefore be a much larger than the shaft. One degree of freedom must be controlled during propagation, which can be achieved using a linear actuator.

1.3 Problem definition

In the future, flexible instruments with follow-the-leader behaviour could be useful for minimally invasive surgery in confined and delicate areas of the human body. A review of state-of-the-art instruments indicates that conserving the shape of the instrument is significantly more difficult than steering and propagation. An interesting novel approach is to conserve the shape in a mechanical shape memory. This mechanical shape memory controls the of orientation of each individual shaft segment through pairs of steering cables. These cables stretch under tension, resulting in damping of the shaft's shape. It is therefore interesting to incorporate a mechanical shape memory inside the shaft, as this could avoid the shape damping effect caused by the use of cables. Current mechanical shape memories are rigid across their length and are therefore not suitable for placement inside a flexible shaft. They are also complex, which makes miniaturization to fitting dimensions for minimally invasive surgery challenging.

1.4 Research goal

The research goal is to design, prototype, test and evaluate a mechanical shape memory that can be incorporated in a flexible, snake-like shaft. This mechanical shape memory must conserve the shape of the shaft to allow for FTL locomotion. The shaft should have appropriate dimensions for use in minimally invasive surgery (footprint ≤ 10x10 mm, length ≥ 150 mm). The prototype is to be tested on a curved path to establish its ability to move forward with FTL locomotion.

1.5 Report structure

The state of the art is described in detail in section 2. Three shape memory concepts are proposed in section 3, which are compared, and one is chosen to be used in the final design. This concept is further refined in section 4 to include a sliding mechanism. The final design is described in section 5. Two prototypes were made, and their fabrication, assembly and testing are described in section 6. The design is further discussed and recommendations for future research are given in section 7. The conclusion of this research is reported in section 8.

2 Analysis

2.1 Design aspects

Propagation

The propagation of the device concerns the advancement of the instrument into, or out of, the body. Two types of propagation are recognized in literature, namely shifting and deploying [15]. In shifting propagation, all segments of the shaft propagate over the same distance at the same time [25]. In deploying

propagation, only the distal part of the shaft advances. A number of FTL instruments does not fit either definition, therefore a new categorization is proposed, illustrated in Figure 4.

The two main types of propagation are shifting and deploying. Shifting propagation is subdivided into synchronous and asynchronous propagation. Deploying propagation is subdivided into telescopic and elongation. The definitions are as follows:

- **Shifting**: All segments of the shaft advance over the same distance.
  - **Synchronous**: All segments advance simultaneously.
  - **Asynchronous**: Segments advance asynchronous.
- **Deploying**: The proximal end remains stationary while consecutive segments advance.
  - **Telescopic**: Segments advance by sliding out of/over preceding segments.
  - **Elongation**: Segments advance through lengthening.

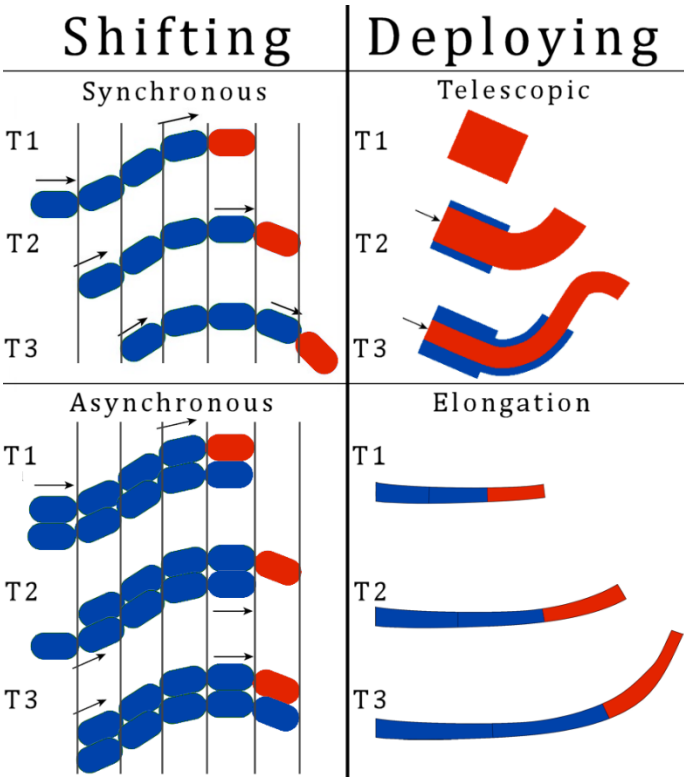

Figure 4: Illustration of distinct types of propagation in FTL instruments. The leader segment is illustrated in red, follower segments in blue. Two main types of propagation are shifting and deploying. In shifting propagation, all segments of the shaft advance over the same distance, either synchronously or asynchronously. In deploying propagation, the proximal end remains stationary while the consecutive segments advance. This may be done telescopically, or by elongating the segments. Adapted from [26].

Steering

An FTL instrument is steered by changing the orientation of the leader with respect to the follower. Culmone *et al.* [15] divided steering mechanisms in state-of-the-art instruments into six categories:

1. Rotary actuators
2. Cables
3. Elastic relaxation force
4. Shape-memory alloy (SMA)
5. Electromagnetic force
6. Hydraulic force

Several instruments contain rotary actuators to steer the leader, which are embedded inside the shaft [26][27][28]. The smallest device is designed by Chen *et al.* [26], which has a diameter of 15mm. This instrument contains two rotary actuators that steer the leader in 3D. These actuators are 6mm in diameter and lie adjacent to each other, contributing significantly to the outer diameter of the device. Actuators of this size deliver little torque, therefore they added several gears and a transmission. This increased the length of each segment to 35mm. Their device is thin enough to fit through multiple natural orifices such as the mouth and anus but is too large for endonasal surgery. Actuators with a diameter of 3mm are commercially available [29], leaving room for further miniaturization.

Steering cables are used in many devices (e.g. [17],[30],[31]) and offer a simple, compact and inexpensive solution compared to embedded actuators. The cables run from the leader to the control module and can be pulled to change the curvature or orientation of the leader. The pulling force may be applied manually or through actuators. A tiny device using cables for steering is designed by Gao *et al.* [31] and has a diameter of 3.4 mm.

Elastic relaxation forces are used to steer so-called concentric tube robots. These robots consist of compliant pre-curved tubes, as illustrated in Figure 5. When these pre-curved tubes are placed in each other concentrically, they deform until the elastic forces the tubes apply onto each other reach a stable equilibrium. This is demonstrated in Figure 5, in which Tube 1 is pre-curved to the left and Tube 2 is pre-curved to the right. Placing Tube 2 inside Tube 1 results in a straight shape. To steer this device, one of the tubes is rotated with respect to the other tube. This changes the direction of the pre-curve, causing the shape of the two tubes to change to reach a new force equilibrium. It is also possible to use one tube for steering, but only if the curvature of the tube matches the shape of the path.

Shape memory alloys (SMA) are a type of material that can be deformed at a cold temperature and return to their original shape when heated. It is commonly used in the shape of a wire. This SMA wire is then placed in an elongated position, and when heated it will shrink to its original size, generating a pulling force. It is used in two

designs to steer the leader [25][32]. Ikuta *et al.* [25] designed an endoscope, 13 mm in diameter, and integrated a water-cooling system to cool down the SMA wires after each actuation. This decreases the time between steering operations, allowing the instrument to propagate faster.

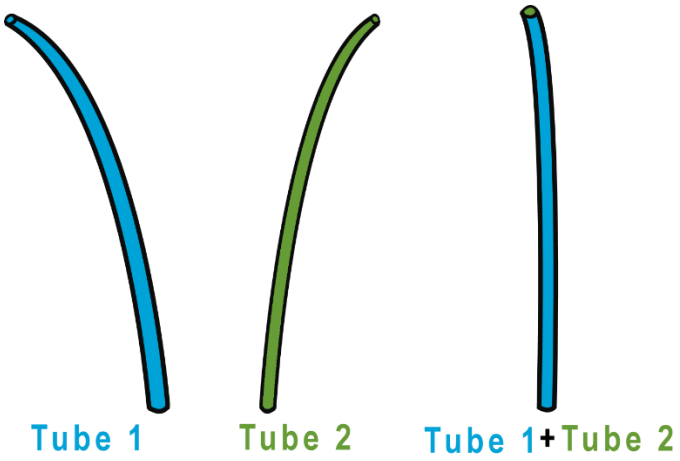

Figure 5: Illustration of the working principle behind concentric tube robots. These robots consist of pre-bend tubes which fit into each other concentrically. The tubes together obtain a new shape, intermediate between the shape of the individual tubes. By rotating one tube with respect to the other tube, the shape can be changed to steer the robot.

Electromagnetic force is used in the device of Tappe *et al.* [33][34]. Each segment pivots around a revolute joint, as displayed in Figure 6. The segments are bi-stable and can switch between the two orientations through electromagnetic forces. The segments, shaped like disks, contain embedded coils on each side of the joint. An electromagnetic force is generated when electricity runs through the coil, causing the segment to hold its orientation or switch to the other orientation. Each segment has only one degree of freedom. The joints of each segment are perpendicular to the joints of its neighbouring segments, allowing the device to move in 3 dimensions. The leader in this design consists of two segments to steer the device in 3 dimensions.

One device uses hydraulic force to steer the tip [35]. The device has three water jets perpendicular to the shaft. By controlling the flow rates of these jets, the tip can be steered. Using water jets for steering is not an ideal solution as it interacts with the surrounding tissue.

Conservation

When an instrument with shifting propagation is moved forward, the shape is propagated backwards. This requires that the position of each segment is copied and then transferred to the previous segment. This can be done through either software (a computerized controller) or hardware (a mechanism).

In software solutions, 1 actuator per DOF is required to control the shape of the instrument. As an FTL instrument has a large number of DOF, many actuators are required, making this an expensive solution. Actuators can be placed inside or outside the shaft, the latter is done more frequently. When actuators are located outside the shaft, they are connected to the follower segments through cables.

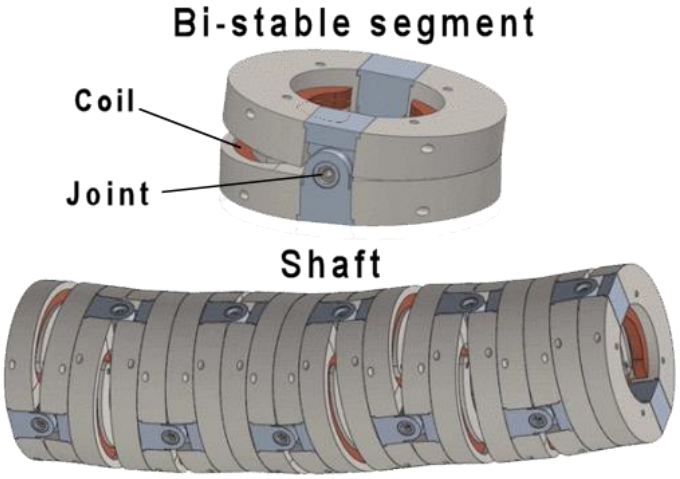

Figure 6: FTL instrument by Tappe et al. [33]. *This instrument uses electromagnetic forces to change the orientation of individual segments. The axis of rotation of each segment is perpendicular to those of the neighbouring segments, allowing the device to move in 3D.*

Two research groups have indicated that friction between the cables and the shaft is a problem that causes the shape of the shaft to be dampened [17][31]. They found that for single curvatures, the deviation between the desired path and measured path is larger at larger bending angles. The deviations are also larger when two curves are in opposite directions (S-curves). The friction between the cables and the shaft depends on the shape of the shaft, with larger curvatures resulting in more friction. With increased friction, more tension in the cables is required. The variable tension in the cables causes two unwanted effects. First, the cables stretch under tension, and the amount of stretch depends on the material's stiffness (Young's modulus) and diameter of the cable. The cables have a small diameter to fit into the shaft and must be flexible enough to follow the curvature of the shaft. These factors limit the maximum stiffness of the cable. A control module would have to compensate for the cable stretching [17]. Secondly, tensioning of the cables results in an internal force that attempts to straighten the shaft [18]. Conserving the shape is therefore difficult when cables are used.

Another group of FTL instruments contains a conservation mechanism that physically constraints the motion of each segment so that they can only adopt the position of the previous or next segment during propagation. These conservation mechanisms can be placed outside the shaft (similar to a control module) or can be integrated in the shaft.

The MemoFlex II has a conservation mechanism outside the shaft. Figure 7 illustrates how his instrument works. In this design, cables connect each segment of the shaft to an individual node in a control module. These nodes fall into a fixed physical track. When the instrument moves forward, the control nodes slide through the track. This way, FTL locomotion is obtained.

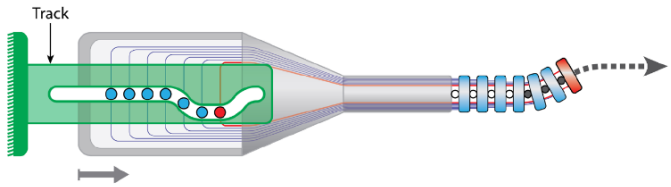

Figure 7: Conceptual illustration of the MemoFlex II FTL instrument controlled through a stationary track [17]*. Cables run from each shaft segment to a node in the control module, which fall into a physical track. When the instrument moves forward, the nodes slide through the track, resulting in the shape being shifted backwards.*

Henselmans *et al.* [12] designed a conservation mechanism called the MemoSlide, which is displayed in Figure 8. The MemoSlide contains two rows of segments, with the left row forming a memory bank and the right row containing a steerable leader segment and a number of follower segments. Each segment has one degree of freedom and can move left and right. This degree of freedom can be blocked by a locking bar. One locking bar is positioned above each row of segments and controlled through a cam with a varying height profile. The segments of the memory bank lie adjacent to the segments on the right. Through a set of wedge-shaped grooves, the positions of the leader and follower segments copied to the memory bank. The memory bank can slide down over the width of one segment. To obtain FTL motion, the shape contained by the leader and follower segments must shift downwards. This can be done by executing a specific sequence involving the locking and unlocking of each row and the sliding of the memory-bank. Starting from the initial position in Figure 8 with both rows unlocked, the order is as follows:

1) Lock the memory bank.
2) Slide the memory bank down.
3) Lock the right row.
4) Unlock the memory bank.
5) Slide the memory bank up.

This set of operations can be repeated and is reversible.

The key advantage of the MemoSlide is that the shape is accurately preserved through many repetitions. This is due to the use of geometrical locks, which makes the positions of each element discrete and prevents the shape from being lost over time [24]. A disadvantage is that it has to be connected to the shaft segments through cables, which brings the problems of cable stretching and shaft straightening along. The MemoSlide cannot be embedded in the shaft itself because it has several rigid elements (e.g., the locking bar and frame) in the axial direction. The maximum deviation of each element is limited as all elements are locked with respect to the locking bar.

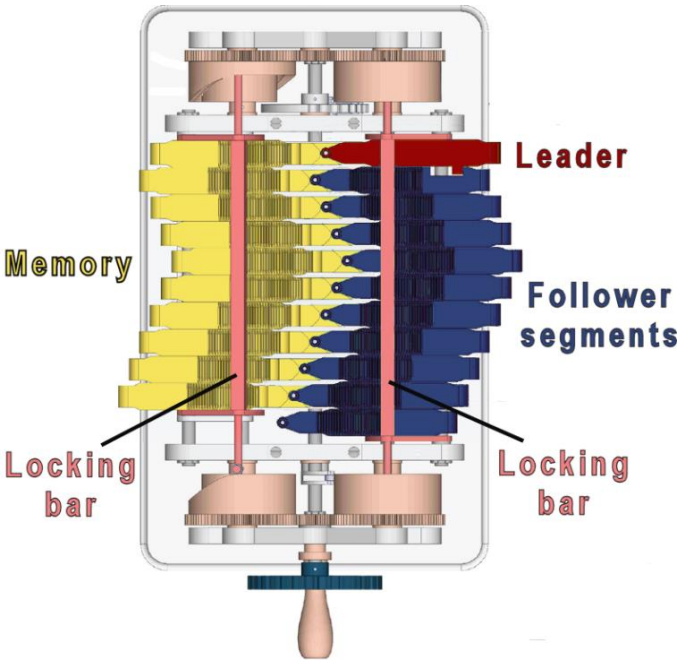

Figure 8: Illustration of a 2D shape-memory device called the MemoSlide. It contains two rows of segments. One row contains the leader and follower segments, the other row memory segments. Through a series of operations, the shape maintained by the leader and follower segments is conserved. Adapted from [12]*.*

The shape is conserved inside the shaft in a branch of FTL instruments called alternating instruments. These instrument consists of two shafts which alternate between a flexible and rigid state [18][19]. When one shaft is rigid, it functions as a physical guidance to the flexible shaft. The flexible shaft can then advance and be steered into a new direction before turning rigid. This cycle is continuously repeated. At any point in the cycle, one of the two shafts is rigid to conserve the shape of the instrument. A commercially available instrument based on this principle is the Highly-Articulated-Robotic-Probe (HARP), which has a diameter of 12mm [19]. Its schematic operation is illustrated in Figure 9.

The HARP uses cables to pull segments of the shaft against each other, creating enough friction between the segments that turn the shaft rigid. Yikilmaz *et al.* found that the use of cables is not an ideal approach, as tensioning the cables result in an internal force that wants to straighten the shaft [18]. Additionally, friction is not reliable for accurately holding the shape of an instrument over a large number of cycles. Through the course of many cycles, minor amounts of slipping will result in the shape being lost. Therefore, Yikilmaz *et al.* designed an alternating instrument using pneumatics to actuate geometrical shape locks that turn the shaft rigid. Their

prototype, 40mm in diameter, was not able to hold the shape after 3 cycles as the weight of the shaft would cause slipping in the geometrical locks.

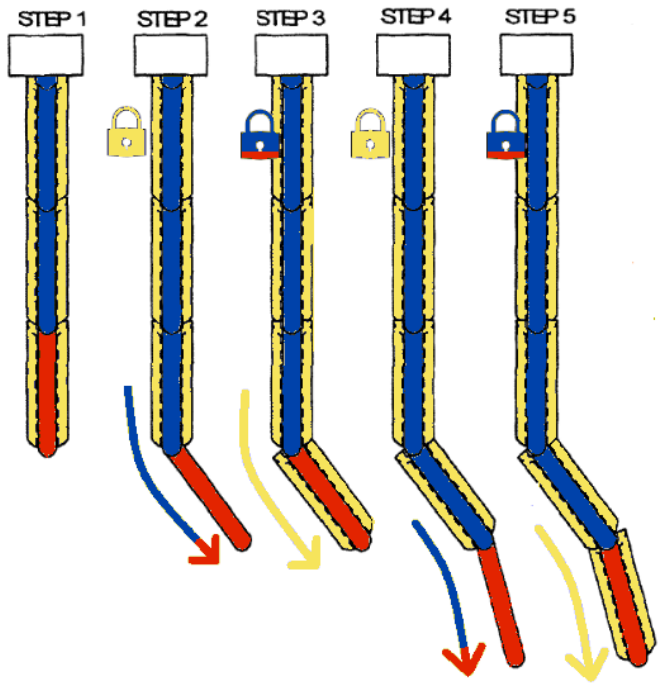

Figure 9: Illustration of the working principle of the Highly-Articulated-Robotic-Probe (HARP). The leader segment is coloured red, the follower segments blue, and the memory segments yellow. This instrument is an alternating device, consisting of two concentric shafts. Each shaft can switch between rigid and flexible states, illustrated with locking symbols. Through the illustrated series of operations, the robot achieves FTL locomotion. Adapted from [20].

In instruments with telescopic deploying propagation, only the leader moves forward whereas the follower segments remain stationary. The shape is conserved in the follower segments. As the followers are stationary, their shape does not need to be shifted backwards to obtain follow the leader locomotion. Instead, they need to hold their shape during every propagation cycle, as illustrated in Figure 10.

In concentric tube robots, the shape is held through elastic relaxation forces. For the case illustrated in Figure 10, the shape of the first segment has to be conserved by elastic forces of tube 1, tube 2 and tube 3. In the second segment, the shape is conserved by tube 2 and tube 3. As tube 3 is the leader, it could be rotated for steering and is translated for propagation. In both cases, the elastic forces applied by tube 3 on the other two tubes changes. To compensate for this, the follower tubes must be rotated during both steering and propagation to conserve the shape. To do so accurately, computer models are required and the entire path of the instrument is planned in advance [24]. Gilbert *et al.* [36] found that pure FTL locomotion in concentric tube robots is only possible in three cases. For two concentric tubes:

1. One tube has a pre-curvature, the other tube does not have a pre-curvature.
2. Both tubes have a circular pre-curvature, and curve in either the same or the opposite direction.
3. Both tubes have a helical pre-curvature and have equal helical torsion. They curve in either the same direction or in opposite direction.

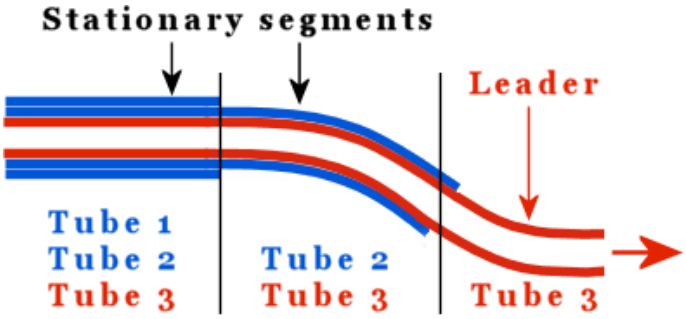

Figure 10: Illustration of a concentric tube robot consisting of three tubes and three segments. The stationary segments on the left conserves the shape, while the leader tube (Tube 3) is deployed and can be steered. Tube 3 runs through the stationary segments and also applies an elastic force on the other tubes. Rotating and/or translating Tube 3 therefore changes the applied forces in those segments. This makes conservation of shape in this type of instrument difficult.

2.2 Overview of solutions

Different solutions for propagation, steering and conservation are discussed in previous paragraphs. The ACCREx tree, displayed in Figure 11, illustrates which solutions can be combined. It contains solutions found in literature and hypothetical solutions. The propagation method determines the structure and movement of the instrument and therefore has a large influence on the steering and conservation methods.

In telescopically deploying mechanisms, the segments must fit into each other, leaving little to no space for any type of actuator. Therefore, these are mostly concentric tube devices, either using elastic relaxation or cables to steer. Only one documented instrument uses elongation deployment [37], which uses cables for steering. The segments must elongate significantly during propagation, therefore it is impractical to place any type of actuator inside the segments.

In synchronous shifting mechanisms, each segment must be actuated. This can be done by cables that connect the segments to a control module outside of the shaft, or by placement of an actuator in the shaft. In the latter case, software is needed to control the actuators. Asynchronous shifting mechanisms can be steered using cables or actuators, while the shape is conserved by friction or interlocking geometry in each segment of the shaft.

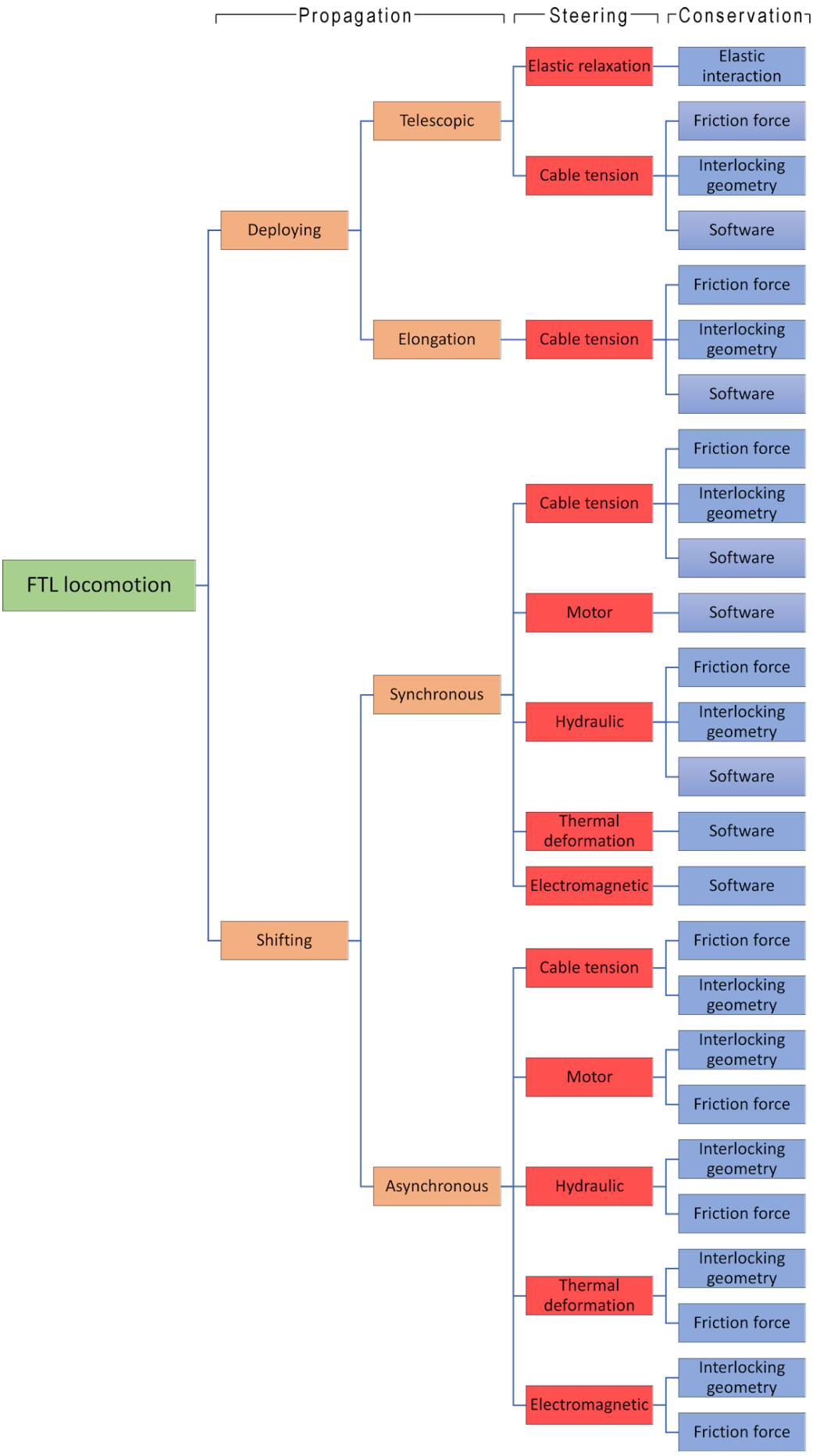

Figure 11: Overview of solutions for FTL locomotion, displayed in an ACCREx tree. Propagation methods are indicated in brown, steering methods in red and shape conservation methods in blue.

3 Conceptualisation

3.1 Requirements

The requirements are split up in three categories: functional requirements, performance requirements and dimensional requirements. The design must comply with the following functional requirements:

- The shaft has to propagate and retract with follow-the-leader locomotion.
- The tip of the shaft can be steered in two directions (left and right).
- The shaft must be able to deflect in alternating directions in one plane (e.g. obtain an S curve)
- The shaft has to propagate, conserve the shape and steer using forces applied from the control unit.

The design assignment is explorative, hence there are no performance requirements relating to one specific minimally invasive surgical procedure. Instead, there are several generalised performance requirements that make the design feasible for use in minimally invasive surgery. These performance requirements are:

- The shaft deflection falls in the range of 30 to 90 degrees per segment.
- The shaft must be stiff to allow surgical tools, such as cutting tools, to be added to the tip. Typical cutting forces to cut through soft tissue (2-8 N) may not cause more than 10% bending of the shaft.

The required minimal shaft deflection depends on the path it needs to follow, which is specific to the minimally invasive surgical procedure. A shaft deflection of 30 degrees per segment could make it useful in some surgical procedures. Larger deflections of up to 90 degrees per segment are expected to further increase its potential use cases.

The shaft should be stiff to allow cutting tools to be added to the tip to cut through soft tissue without causing the shaft to bend more than 10%, as larger deformations are more likely to cause the instrument to collide with surrounding tissue. Typical cutting forces to cut through soft tissue fall in the range of 2-8 N [38].

The ten thinnest state-of-the-art devices reported in the literature review of Culmone *et al.* [15] have diameters ranging from 0.40 mm [39] to 7.0 mm [40] and length/diameter ratios ranging from 10 [37] to 45 [41]. Five of these designs are concentric tube robots [42][41][43][44][45], which can obtain a limited number of shapes which limits their use cases [36]. The other five designs make use of cable tension [39][31][16][46][40]. The friction between cables and shaft results in positional errors depending on the curvature of the shaft [17][31][47][48]. Therefore, a design able to follow a wider range of paths than current concentric tube robots without suffering from the positional errors of current cable actuated instruments is competitive with the state-of-the-art devices and forms a solid addition to them. The dimensions of the design should be close to the dimensions of these state-of-the-art devices. Because the design's FTL capabilities should be an improvement over state-of-the-art devices, the dimensional requirements are more relaxed. The dimensional requirements are therefore as follows:

- The maximum shaft width is 10 mm.
- The maximum shaft height is 10 mm.
- The minimal shaft length is 150 mm.

3.2 Solution space

The ACCREx tree, presented in Figure 11, is used to find a solution space that meets the requirements. Deploying telescopic solutions consist of segments that either fit into each other concentrically or lie parallel, which limits the volume of the individual segments. For example, in concentric tube robots, each successive tube has a smaller diameter and thus less volume than the previous tube. Therefore, the maximum stiffness of the segments decreases towards the distal end. This solution is therefore not ideal to obtain a high shaft stiffness.

Deploying elongating solutions consist of segments that increase in length to propagate forward. FTL locomotion is difficult to obtain with this type of instrument. When a segment elongates, it must follow the path that was previously held by multiple segments. For example, suppose there are two segments bent in alternating directions forming an S curve. If the segments are elongated to twice their initial length, then one segment must obtain the S curve previously held by the two segments. Segments can only obtain shapes with multiple curves if they have multiple degrees of freedom along their length. This makes the segments more complex and the control task difficult.

Synchronous shifting solutions consist of a column of segments in which each segment has its own controllable degree of freedom. There are multiple methods to control the degree of freedom. One method is to use cable tension. However, the friction between the cable and the shaft results in positional errors depending on the curvature of the shaft [31][47][48][17]. It is therefore not ideal to use cable tension to obtain FTL locomotion. Alternative methods to control the degrees of freedom make use of actuators embedded in the shaft. Small electromechanical actuators are still large with respect to the diameter of the shaft [29] and motor malfunctions have occurred in at least one clinical study [49].

Asynchronous shifting solutions consist of two concentric or parallel shafts which alternate between a rigid and flexible state. Because the shape is conserved by the rigid shaft, these solutions require a minimum number of actuators [15]. The segments of the shaft can be stiff, with the DOF achieved through joints between the segments [50]. This solution is therefore a good option to obtain a high stiffness. Asynchronous shifting solutions are thus most likely to fulfil the requirements.

There are several steering options for asynchronous shifting solutions. Steering cables are the simplest and least expensive option. The shape can be conserved through interlocking geometries or through friction forces. Interlocking geometries are the most reliable option to conserve the shape over time, because they are less likely to slip.

3.3 Hierarchy of an asynchronous shifting instrument

The hierarchy of the shaft of an asynchronous shifting instrument consists of 3 levels (high to low):

1. The shaft, consisting of two parallel or concentric memories.
2. The memories, consisting of a column of segments.
3. The segments, which can alternate between a rigid and flexible state and consist of:
    a. A leader, which is the steerable segment at the distal end of the memory.
    b. Followers, which follow the path of the Leader.

The functions of the shaft segments are simpler than the functions of the entire shaft. Therefore, a bottom-up design approach is used to simplify the overall design process. This bottom level of the design consists of the segments, and their functions are to be defined. The two types of segments are the leader segment and the follower segment, which have almost identical functions.

The leader segment has the following functions:

- Have 1 Steerable DOF.
- This DOF can be locked and unlocked in multiple positions, actuated by its adjacent follower segment.
- When unlocked, this DOF can be steered from the control module.

The follower segments have the following functions:

- Have 1 DOF.
- This DOF can be locked and unlocked in multiple positions, actuated by its proximally adjacent segment.
- Propagate the locking/unlocking actuation to the next segment.

The segments together form the memory. The memory has additional functions:

- Slide axially with respect to the other memory over an integer number of segments.
- Align with the other memory at the start and end of the sliding motion.

3.4 Segment concepts

Introduction

There are different options to obtain one DOF in each segment (e.g., hinges, sliders). Because these joints have different motions, they have a strong influence on the rest of the design. The joint type is therefore used as a starting point to create three designs that are vastly different from each other to obtain an innovative design. This approach was fruitful, as early in the concept generation stage an interesting and innovative concept was found.

There are two types of joints with one DOF, revolute joints (hinges) and prismatic joints (sliders). Three conservation concepts are proposed, one with a hinge, one with a slider, and one with multiple hinges. One of these concepts is chosen to form a basis of the final design. Steering is not considered in these concepts, as it only applies to the leader segment and is expected to be relatively simple. A steering concept is discussed in section 7.4.

The Lateral Slider

The Lateral Slider is displayed in Figure 12 and has a slider in each segment. Each segment can move laterally with respect to the surrounding segments. The slider consists of a T-shaped rail on top of each segment that falls into a T-shaped notch at the bottom of its neighbouring segment (Figure 12).

Each segment contains a vertical locking bar which has a geometrical lock on top and a square-shaped plate at the bottom (Figure 12a, indicated in green). The bottom of each segment contains another geometrical lock (Figure 12b, indicated in red). The locking bar can slide up and down with respect to the segment. When it is pushed upwards, the geometrical lock on top of the locking bar falls into the geometrical lock at the bottom of the next segment, locking the two segments together (Figure 12c). The top of the locking bar also presses against the bottom of the next locking bar, pushing it upwards. This way, the locking motion is propagated through the segments, causing all segments to lock simultaneously. Locking can be controlled from the bottom segment. The locking plate is rectangular in shape

to ensure an overlap exists between the plate and the bottom of the next shaft segment.

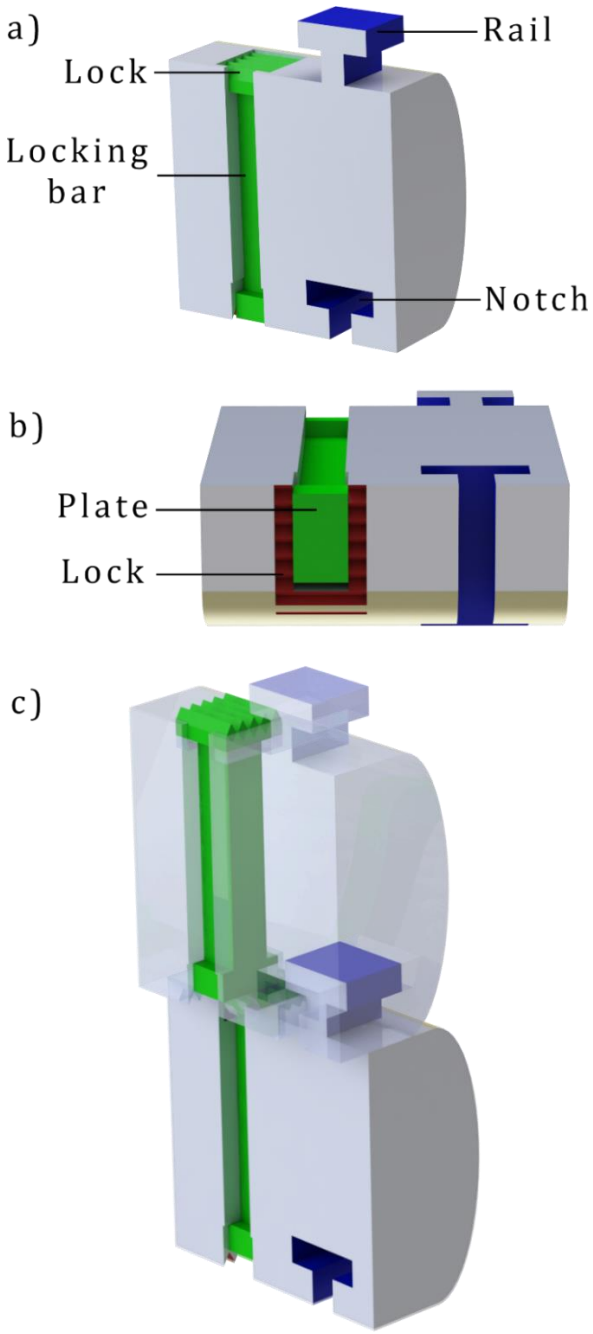

Figure 12: Illustration of The Lateral Slider, rendered in SolidWorks [51]*. Part of the main body was made transparent to increase visibility on the internal mechanism. a) Isometric view of a single memory segment with its parts labelled. b) Bottom view of a single memory segment, displaying the plate (green) at the bottom of the locking bar and the locks (red) embedded in the segment. c) Isometric view of two memory segments. The locking bar is pushed upwards to lock the position of the top segment with respect to the bottom segment.*

The Rotator

The Rotator is displayed in Figure 13. Each segment has a revolute joint, which attaches to a link connected to the next segment (Figure 13a). As the link rotates around the joint, the segments change orientation with respect to each other. Each body has a convex shaped front side and concave shaped back side, both with the same radius. This allows the front side of one body to slide over the back side of the next body during rotation, increasing the stiffness of the design.

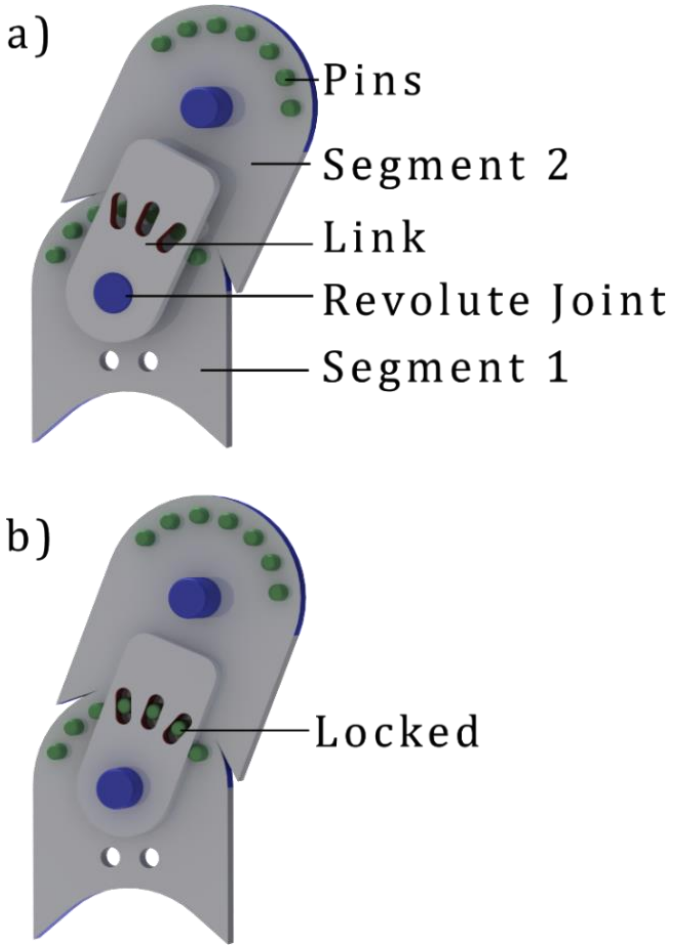

Figure 13: Illustration of The Rotator, rendered in SolidWorks [51]*. a) Two memory segments with their parts labelled. Segment 2 attaches to the link and can rotate over the revolute joint. A row of pins surrounds the revolute joint. b) The two memory segments are locked together by pushing the link towards the segments. The slots of the link fall into the pins, locking the position.*

Each body has a row of pins at a constant radius around the revolute joint. The link has three slots in which the pins of the segment fit. When the link is pushed against the two bodies, the pins fall into the slots locking the orientation of the body (Figure 13b). To actuate locking, a pneumatic system could be used. An air tube can run past the links, compressing the links and segments together when the tube is pressurized.

The Shearer

The Shearer uses a number of hinges per segment. Each segment contains two connected parallelograms forming a linkage mechanism, which can shear sideways while the top and bottom of the segments remain parallel to each other, as displayed in Figure 14. Because the bottom and top links remain parallel, the sideways

deviation of one segment does not cause rotation of the next segment, only translation.

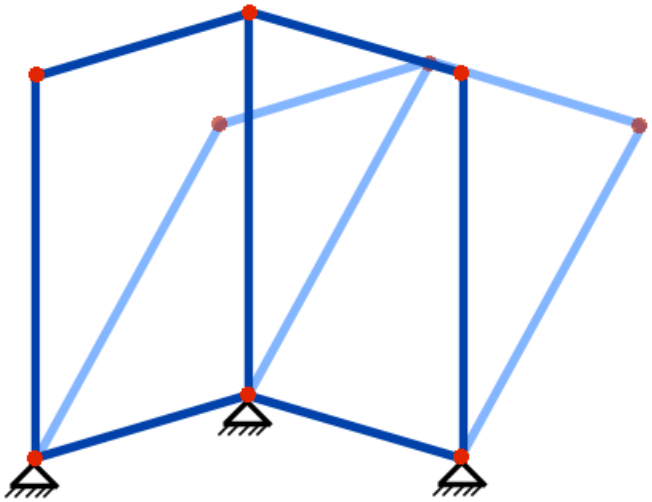

Figure 14: Illustration of The Shearer. Each segment consists of two connected parallelograms, resulting in a single DOF, allowing the segment to shear sideways. Links are indicated in blue, joints in red. The dark coloured elements show the mechanism in a neutral position, whereas the light blue elements show the mechanism in a sheared position.

The mechanism as shown in Figure 14 is expanded to include a locking mechanism as shown in Figure 15a. Two new links are added, indicated by the yellow colouring, connected through a joint. Rows of geometrical locks are added, pointing downwards on the yellow links, and pointing upwards on the bottom blue links, indicated in Figure 15 with triangles. To be able to lock and unlock, an additional degree of freedom is added by connecting the two bottom joints to sliders, allowing the mechanism to be compressed and decompressed. When the two bottom joints are compressed, the yellow and blue geometrical locks are pushed into each other, as illustrated in Figure 15b. This locks the position of the segment, turning the segment into a rigid structure. The segments can lock in a range of positions, as displayed in Figure 15c.

The segments can be stacked on top of each other to create a longer mechanism, which is displayed in Figure 16. When the bottom nodes of the bottom segment are compressed, all other segments are also compressed. This occurs because the top and bottom links of each segment always remain parallel to each other, resulting in the compression of the first element being propagated to all subsequent segments. This means that virtually an infinite number of segments could be added, and a single compression at the bottom would still lock all segments. In reality play in the joints can cause a dampening effect, limiting the number of segments that can lock simultaneously through one actuation movement.

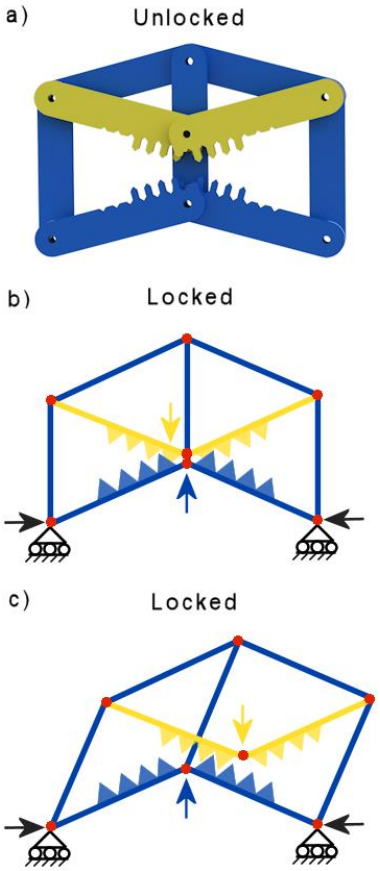

Figure 15: Schematic illustration of the locking mechanism of The Shearer. a) The mechanism in an unlocked state in neutral position, allowing shearing deformation. Rendered in SolidWorks [51]*. b) The mechanism in a locked state in neutral position. Compression of the sies (dark arrows) results in the lower (blue) lock and upper (yellow) lock moving into each other. c) The mechanism locked in a deformed state.*

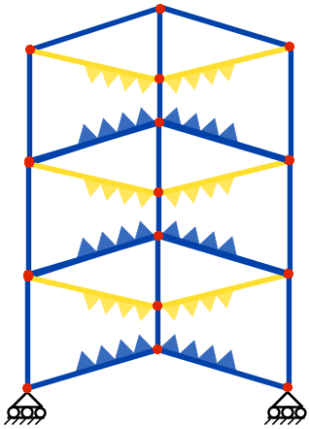

Figure 16: Illustration of The Shearer with three memory segments stacked on top of each other. The top links of one segment will form the bottom links of the next segment.

3.5 Segment concept selection

Selection criteria

The three concepts were compared based on five criteria. The first criterion is the feasibility of a concept. Feasibility is the measure of how realistic it is to build and test a design within the limits imposed by a master's thesis. The second criterion is the shaft deflection. A larger shaft deflection is desirable as it allows the

instrument to follow a wider range of paths. The third criterion is the stiffness of a concept. The shaft must be stiff enough to allow surgical tools to be added to the tip. The fourth criterion is the expected cost of a concept, as a cheaper concept is more likely to be an economically viable solution. The fifth criterion is the minimal width of a concept, which is a measure as to what extent the width of a concept can be minimized.

Concept choice

The concepts and criteria are placed in a Harris profile, displayed in Figure 17. Each concept is scored on a four-point scale.

The Lateral Slider is relatively simple and has only two parts per segment. These parts have complex 3D shapes which are difficult to manufacture. Assembling this concept is also challenging, because the locking bar lies within the main body of the segment. Overall, this concept is feasible, due its low number of parts and simplicity of the concept. The rotator requires pneumatic actuation to lock the segments. This makes it more difficult to manufacture and assemble the design. Furthermore, making the pneumatic actuation reliable to actuate locking in every segment is an additional challenge. Therefore, the concept received a lower score for its feasibility. The Shearer contains 2D parts that are simple to manufacture. The entire memory is a linkage mechanism that can be actuated by hand, making testing of the prototype simple. It is therefore the most feasible concept.

The Lateral Slider has a small shaft deflection, because the range of motion of the sliders is limited. The Rotator has a large shaft deflection, because each hinge joint has a large range of motion. The Shearer has a reasonable shaft deflection, but smaller than The Rotator because the segments shear sideways and cannot rotate with respect to each other.

The Lateral Slider has a low stiffness. The overlap between the rail on top of the segment and the notch of the adjacent segment is small when the segment is displaced to the side, which limits the stiffness of the concept. The Rotator has a high stiffness in the sideways direction, as each segment has a thick joint and thick pin. The Shearer has the highest stiffness. In the locked configuration, the linkages form a triangular structure similar to that of a truss bridge.

The Lateral Shearer is relatively expensive, because its parts have complex 3D shapes and are therefore more expensive to manufacture. The Rotator contains simple 2D parts that can be manufactured easily, but the pneumatic actuation system required to actuate the mechanism is more expensive and increases assembly time. The Shearer contains simple 2D parts that are less expensive to manufacture. Assembly of this mechanism is simple because it only requires the joints to be pressed into the holes of the links. Because all the joints are pointed in the same direction, a press could be used to press all the joints into the links simultaneously, making assembly fast. Therefore, The Shearer is expected to have the lowest cost.

The minimal width of a concept is related to the complexity and the smallest features of its parts. The Lateral Slider contains parts with complex 3D shapes and the locks contain small features. It is therefore difficult to miniaturize. The Rotator and The Shearer both consist of simple 2D parts. The Rotator has a pneumatic system that is more difficult to miniaturize, whereas The Shearer has fine features in the locks. Therefore, they both received the same score.

The Shearer has a positive score on all criteria and is therefore chosen to form the basis of the final design.

4 Concept refinement

4.1 Overview

Two memories based on The Shearer concept must slide over each other axially and align at the start and end of each sliding cycle. Specific requirements for the sliding concepts are described in section 4.2. Three sliding concepts are proposed section 4.3, of which one is chosen in section 4.4 to be integrated in the final design.

4.2 Sliding requirements

First, it must be determined which links of the segments can be used as attachment points for the sliding mechanism. Each segment has three links in the direction of propagation, illustrated in Figure 18, of which either can be used as attachment points. The sliding mechanism should not make the instrument wider. Therefore, the center link is the best candidate to attach the sliding mechanism to, as the available space around the central linkage is symmetrical with equal space on either side. If one of the side links were to be used as an attachment instead, the available space would be asymmetrical and thus inconvenient. Using multiple links as attachment points is also possible. However, as the distance between the three links changes during locking and unlocking, it would make the problem more complex. Using the center link as attachment point is therefore the simplest solution.

Secondly, the range of motion of the sliding mechanism must be determined. For the memories to copy the shape of each other, all segments of the two memories must align accurately. Any error in the alignment of two opposing segments is propagated to other segments. This is illustrated in Figure 19. In this figure, the central links of two memories are illustrated, with links of memory 1 in blue and links of memory 2 in green. The segments have a length L, and an arbitrary angle θ exists between segment 1 and 2. The joints of

	The Lateral Slider				The Rotator				The Shearer			
	--	-	+	++	--	-	+	++	--	-	+	++
Feasibility												
Shaft Deflection												
Stiffness												
Cost												
Minimal Width												

Figure 17: Three design concepts are placed in a Harris profile and compared on 5 criteria. Each concept is rated on a four point scale ranging from -- to ++.

memory 2 are connected to the links of memory 1 through a sliding mechanism, indicated by purple joints. In Figure 19a, the central links of segment 1 of both memories are aligned. In Figure 19b, the central linkage of memory 2 has moved upwards over a distance *H* to align with the central linkage 2 of memory 1. However, when the central link is not pushed all the way up (*H* < *L*), it causes an error (*Error A*) between the two joints. This error then propagates to the next segment, indicated by *Error B*. Through geometry we find the following relationship between these two errors:

$$Error\ B < Error\ A, \quad when\ \theta \neq 180°$$
$$Error\ B = Error\ A, \quad when\ \theta = 180°$$

This indicates that if a small error is introduced in the first segment, this error will propagate and decreases with every angled segment. If the error is introduced in a later segment, the error will propagate towards the base and increase with every angled segment. Since the instrument must be able to contain a large number of segments, a small error close to the tip propagates back and becomes a large error near the base. It is important to avoid these errors from occurring. The range of motion of the sliding mechanism must therefore be equal to the length of the segment.

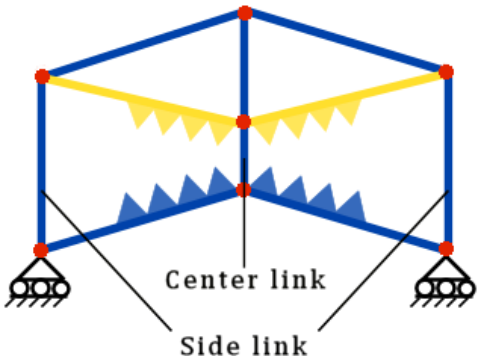

Figure 18: Illustration of a memory segment with its vertical links labelled.

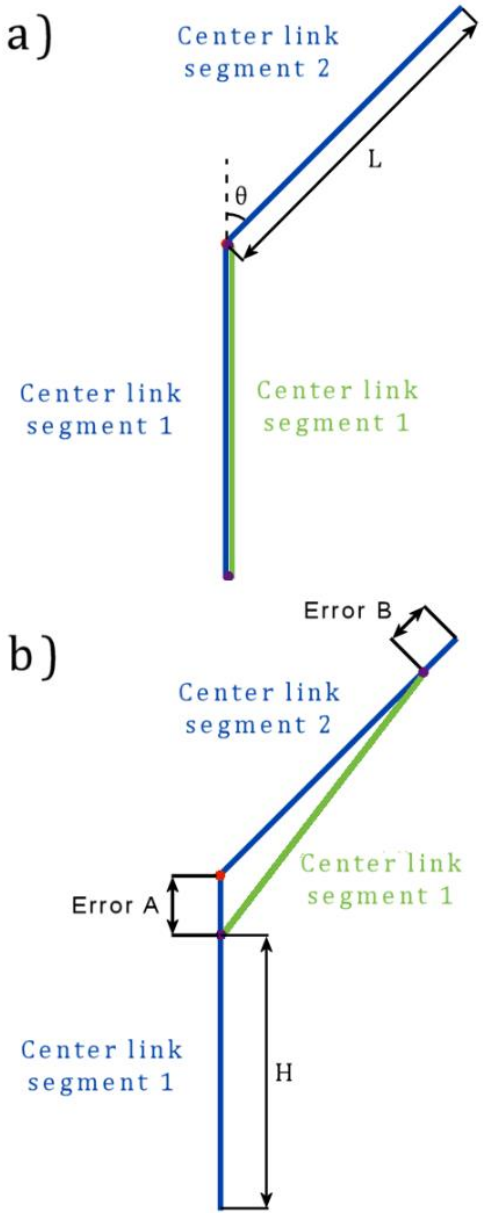

Figure 19: Illustration of the error propagation in the sliding mechanism. Parts of memory 1 are indicated in blue, parts of memory 2 in green. a) The two memories are aligned. Segment 2 is placed at an arbitrary angle θ. b) Alignment errors occur when memory 2 does not slide completely over memory 1.

4.3 Sliding concepts

The Roller

The Roller is displayed in Figure 20. A U-shaped rail is attached to one memory. The second memory has bearings attached to the joints, which can move through the rail. This has the advantage of having low friction. However, it does come with a downside. The rails near the joints contain a gap to allow the joint to rotate. The bearings can move sideways into these gaps, which adds play to the system and increases the force required to slide the memories over each other.

The Wiper

The Wiper is displayed in Figure 21. The blue links are attached to the first memory, the green links to the second memory. The blue links have the shape of an isosceles triangle. The brown link attaches to the lateral corner of the triangle, and its length is equal to the two equal sides of the triangle. The end of the brown link, when rotated around the joint, can reach the other two ends of the triangle. The green links are connected to the end of the brown link. This way, the range of motion of the memory is exactly one segment's length.

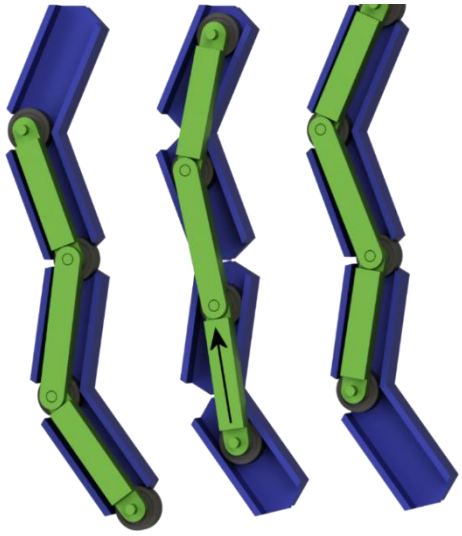

Figure 20: The Roller, rendered in SolidWorks [51]. *A U-shaped rail (blue) is attached to the segments of one memory. The center links of the second memory (green) have bearings attached, which fall into the rail. The bearings can roll through the rail, allowing the memories to slide over each other.*

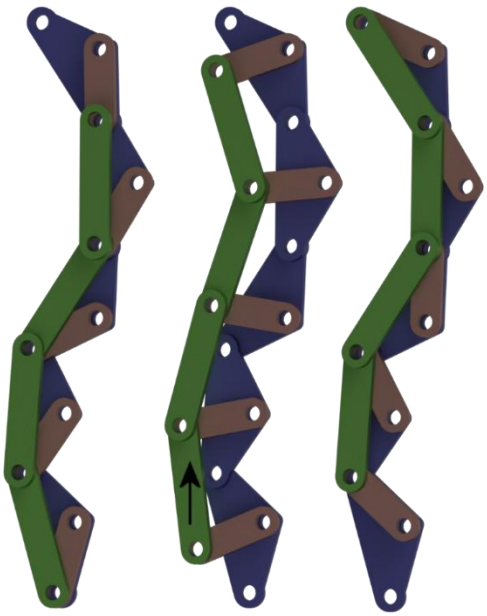

Figure 21: The Wiper, rendered in SolidWorks [51]. *The blue parts connect to the center links of memory 1, the green parts connect to the center links of memory 2. The brown links connect the two memories and allow the memories to move over each other.*

The Ferry

The Ferry is displayed in Figure 22. The center link of one memory is indicated in yellow, which has joints at its distal ends indicated by red dots. On top of the center link lies a slider (blue), which has a long slot in the middle. A pin (green), connected to the center link of the other memory, falls into the slot. This pin can move from one end of the slot (Figure 22a) to the other end of the slot (Figure 22b). When it has reached the end of the slot, it places a force on the slider, which as a results starts to slide over the center link (Figure 22c). When the pin aligns with the joint of the first memory, the bumps at the side of the slider run into the blocks of the center link. The full range of motion of the pin consists of the length of the slot in the slider, plus the range of motion of the slider. Together, the full range of motion of the pin is exactly the length of one segment. The slot of the sliding element ensures that the pin, and thus the joint of the moving memory will precisely align with the joints of the other memory in the end positions.

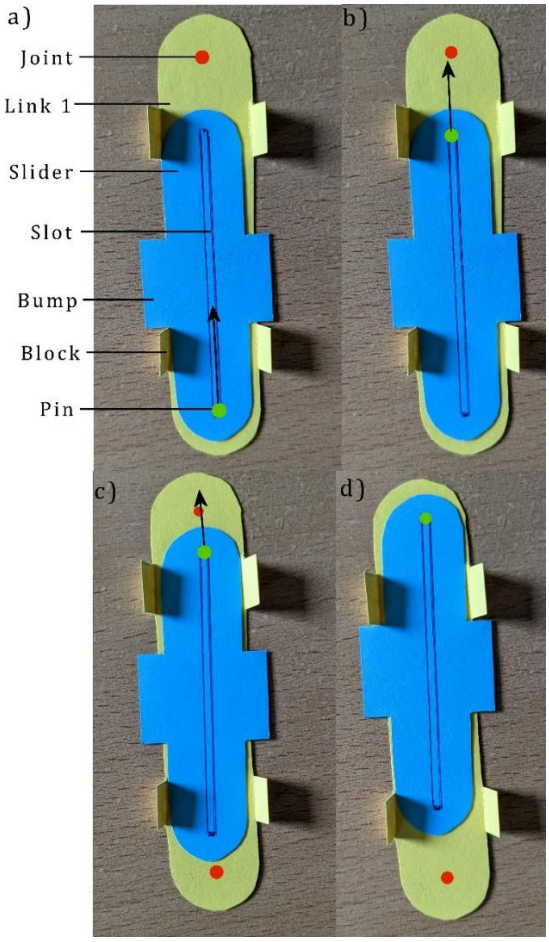

Figure 22: The Ferry, demonstration model made from cardboard. a) The parts of the mechanism labelled. The slider fits between the two memories and rests at the bottom of the center link. The pin (green) aligns with the bottom joint of the center link and is attached to memory 2. b) The pin is pushed to the end of the slot. c) Continuing to push the pin upwards causes the slider to move towards the top of the center link. d) The slider has slid to the top of the center link and the pin now aligns with the top joint.

4.4 Sliding concept selection

Selection criteria

Three criteria were used to select the best sliding mechanism, namely the alignment, friction, and manufacturability. The alignment between the memories is the most important criterion because misalignment will cause the shape to be lost over time. As the two memories will be in sliding contact, friction between the two memories should be low to allow them to smoothly slide over each other. Lastly, the sliding mechanism should be simple to manufacture and assemble. The concepts and the criteria are placed in a Harris profile, displayed in Figure 23.

Sliding concept choice

The Roller aligns well everywhere except at the start and end of the propagation step, where the bearings can fall into the gaps between the rails. Because bearings have little rolling resistance, this concept has the lowest friction. This concept contains a rail, which has a 3D shape without small features, which can be manufactured with relative ease.

The Wiper can align well but cannot do so reliably, because the mechanism becomes bi-stable at some configurations. High friction forces can occur in the joints. The brown links that connect the memories to each other can oppose the actuation force (e.g., Figure 21, second segment from the top), resulting in a larger normal force in their joints. This concept has the highest score for manufacturability because it consists entirely of simple 2D shaped links.

The Ferry aligns accurately at the start and end of each propagation step. There is a sliding contact between the slider and the center link and between the slider and the pin. The friction forces can be reasonably controlled through material selection and lubrication. This concept contains a 2D shaped slider, which is simple to manufacture. The joint containing bumps features some complex 3D geometry but does not contain small features and is therefore still reasonable to manufacture.

The Ferry is the only concept with a good score on every criterion and is therefore chosen to be used in the final design.

	The Roller				The Wiper				The Ferry			
	--	-	+	++	--	-	+	++	--	-	+	++
Alignment												
Friction												
Manufacturability												

Figure 23: Three sliding mechanisms compared in a Harris profile based on three criteria: alignment, friction, and manufacturability.

5 Final design

5.1 Overview

The shaft design, coined the Dullomatic, is shown in Figure 24. The design is 10 mm wide, 8.9 mm thick, and each segment has a length of 15 mm. The shaft contains two memories, which work identically, and a sliding mechanism between the memories connects the two.

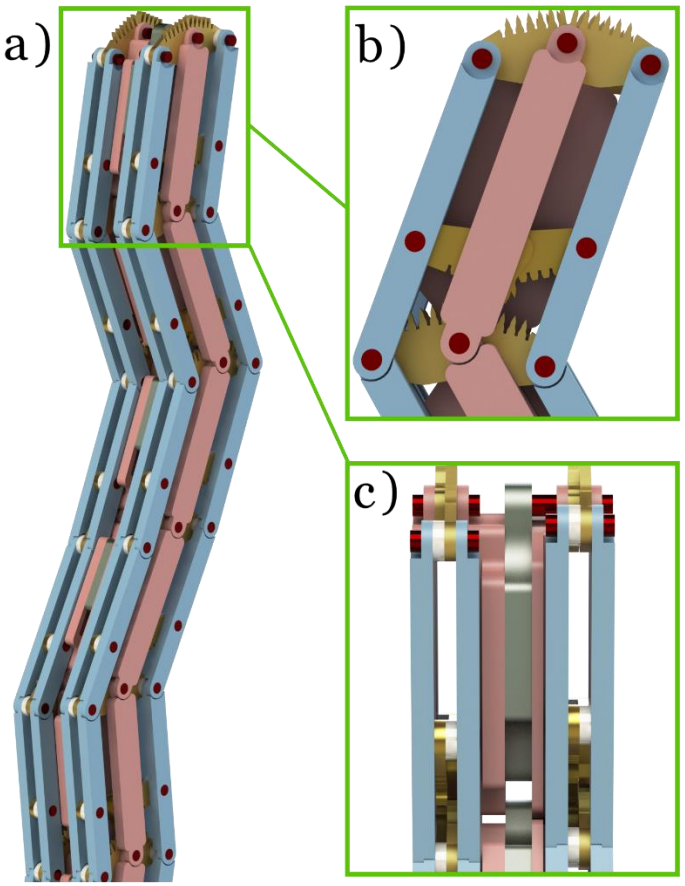

Figure 24: Render of the Dullomatic. a) Overview of the design, showing 2 memories with 5 segments each. b) Front view of one segment. c) Side view, showing the leader segment of two memories and the sliding mechanism in between.

The memory segments are composed of seven unique parts. They contain four types of links (three variations of center link and one side link) and two types of teeth (teeth up and teeth down), as displayed in Figure 25. Dowel pins are used to connect the parts. The sliding mechanism that falls in between the two memories is integrated into the center link on both memories, namely center link plated and center link slots. The number of parts per segment is listed in Table 1.

A full cycle of steering, conserving the shape and propagating is presented in Figure 26. Only one memory advances past the other memory, which will be referred to as the leader memory. The second memory follows the leader memory and is called the follower memory. Locking the shape of the memories is explained in 5.2, and the sliding mechanism in 5.3.

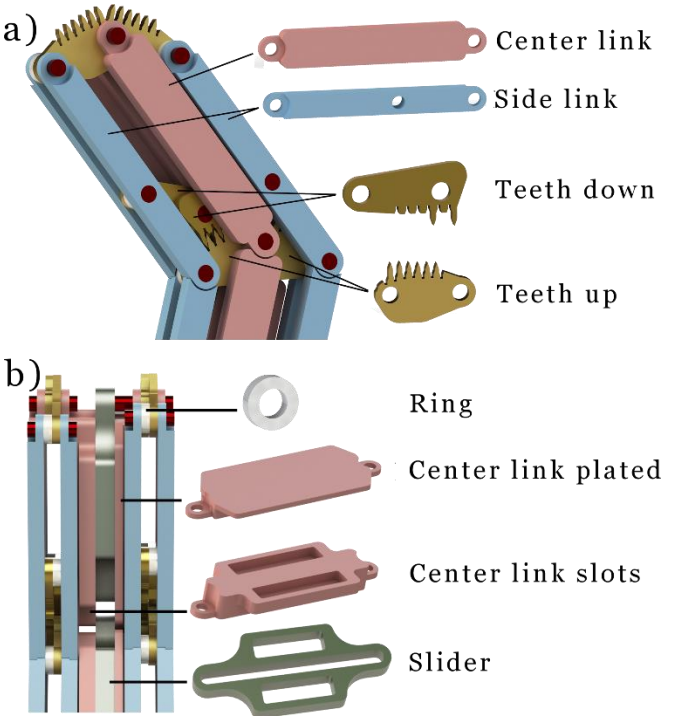

Figure 25: The parts of the Dullomatic. a) Front view of a single memory, indicating the links and teethed parts. b) Side view of the shaft, indicating the parts forming the sliding mechanism.

Table 1: Number of parts per segment of the Dullomatic.

Part name	Number/segment
Center link	2
Side link	8
Teeth down	4
Teeth up	4
Ring	8
Center link plated	1
Center link slots	1
Slider	1
Magnet	4
Dowel pin (1⌀ x 3 mm)	9
Dowel pin (1⌀ x 4.7 mm)	1
Dowel pin (1⌀ x 1 mm)	2

5.2 Shape locks

The memories look complex, but their function is simple. Each memory is either in an unlocked state, allowing each segment to shear, or in the locked state, allowing no deformation. Each memory segment contains a shape lock.

The shape lock is displayed in Figure 27. The mechanism is locked in Figure 27a, and unlocked in Figure 27b. It contains an upper jaw and lower jaw, which are connected to the side links. The lower jaw of each segment is connected to the lower jaw of the neighbouring segments by the center link. Each jaw consists of two links, each containing a row of teeth. The link of the upper jaw can interlock with the link of the lower jaw that lies diagonal to it, forming a diagonal pair. In the unlocked state, the mechanism can shear, which changes the position of the upper jaw with respect to the lower jaw. The upper jaw follows a circular path during shearing, as illustrated in Figure 27b.

The lower jaw has a total of twelve teeth, six on each link. The upper jaw has four teeth, two on each link. This allows the two jaws to interlock in thirteen positions, six on each side, and one middle, neutral position. An overview of the mechanism locking in various positions is displayed in Figure 28.

Three memory segments in the unlocked state are displayed in Figure 28a. The memory is locked by compressing the sides, as shown in Figure 28b. This causes the upper jaws of each segment to interlock with the lower jaws, locking the position of every segment simultaneously. Figure 28c illustrates the unlocked jaws in a side position.

In the side positions, one diagonal pair interlocks. In the most extreme position, displayed in Figure 28d, the first tooth of the upper jaw link falls behind the sixth tooth of the lower jaw link. Adding a seventh tooth on the lower jaw link to encompass the first upper tooth was not possible. Therefore, the upper jaw links contains a second tooth that falls in between two teeth of the lower jaw in this position. The mechanism cannot shear past the extreme position, as the center link will come into contact with the side link blocking further shearing.

In the neutral position, both diagonal pairs interlock, as displayed in Figure 28e. The teeth of the upper jaw links are not completely encompassed by the teeth of the lower jaw links. Instead, the first tooth of the upper jaw link lies adjacent to the first tooth of the lower jaw link. This arrangement constraints shearing motion in only one direction. The diagonal pairs constrain motion in opposite directions, securely locking the neutral position.

The distance between the upper jaw and lower jaw varies slightly depending on the position. This variation arises from the circular range of motion of the upper jaw. To compensate for this, the teeth of the lower jaw have a specific height profile ranging from 0.9 mm to 1.3 mm, allowing the memory segments to lock in every position.

The teeth all have the same width of 0.25mm and the tips have an angle of 20 degrees. The opening between teeth is 0.30 mm, allowing the teeth to interlock smoothly. The opening also has some extra space at the bottom. This ensures that the reaction forces between the teeth in locked position are not placed on the thin tip, but instead on the thicker part of the teeth.

Both the upper and lower jaw links have an irregular outer shape. This increases the surface area between the parts of different layers, which increases the stiffness and lowers the chance that parts of different layers hit each other during operation.

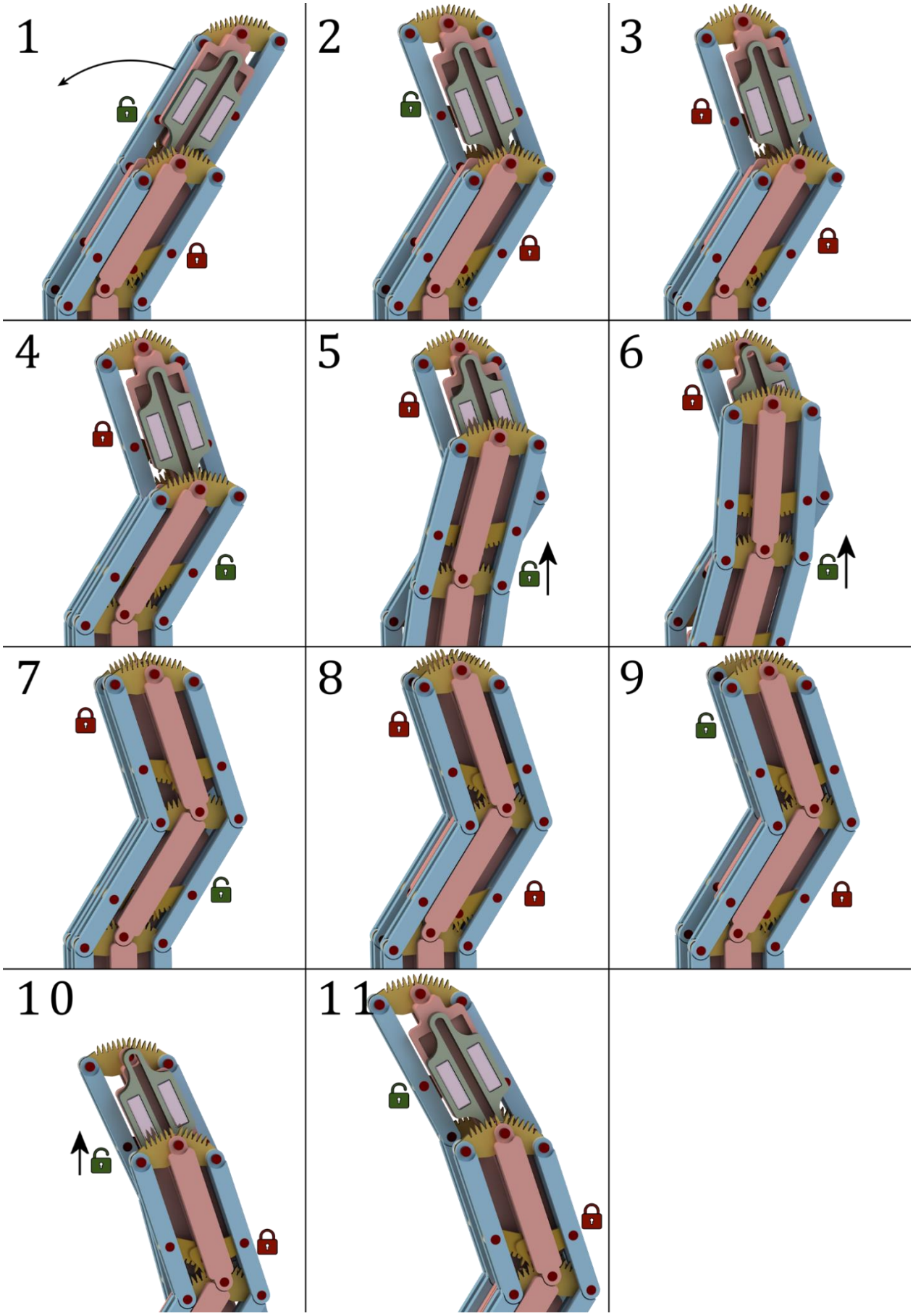

Figure 26: The Dullomatic going through a cycle of steering, conservation and propagating. The memory at the front is the follower memory, the memory behind it the leader memory. Renders were made in SolidWorks. 1-2) Steering the leader to a desired angle. 3) Locking the leader memory. 4) Unlocking the follower memory. 5-7) Sliding the follower memory upwards to align with the leader memory. 8) Locking the follower memory to conserve the shape. 9) Unlocking the leader memory. 10) Sliding the leader memory upwards. 11) The leader can be steered again to repeat the cycle.

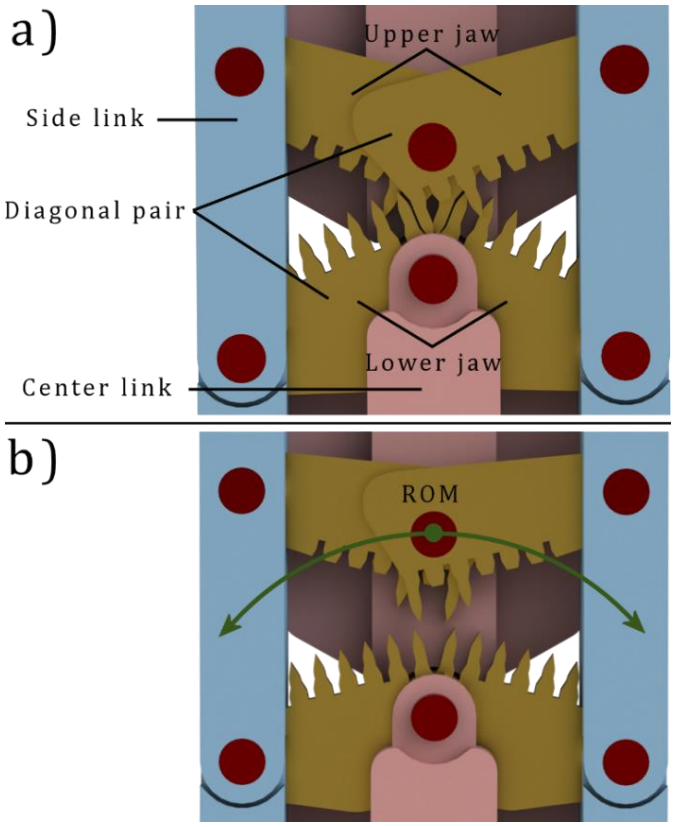

Figure 27: Illustrations of the locking mechanism as present in each memory segment, rendered in SolidWorks [51]*. One center link on the front is made invisible to increase the visibility of the locking mechanism. a) The mechanism in a locked state, with its parts labelled. b) The mechanism in an unlocked state, showing the range of motion of the upper jaw.*

5.3 Sliding mechanism

The sliding mechanism is placed between the two memories and is integrated into the center links of the memories. The mechanism allows the memories to slide with respect to each other over a distance equal to the length of one segment (15 mm). An exploded view of the sliding mechanism is displayed in Figure 29.

A protruding joint at the top of the center link of the follower memory falls into the slot in the middle of the slider. Block magnets fit into the sides of the sliders and fall into two slots of the center links of the leader memory.

The sliding cycle consists of two steps and is illustrated in Figure 30. Only the parts involved in propagation are visible, the rest of the memories are hidden. The two memories are aligned at the start of the cycle, displayed in Figure 30a. During the first step, the protruding joints slide through 12 mm long slots in the sliders, displayed in Figure 30b. In the second step, the sliders slide 3 mm over the center links of memory 1, displayed in Figure 30c. At the end of the second step, the memories are aligned again.

Permanent magnets are incorporated into the sliding mechanism. These magnets fit into the slider, and slide through the slots of the center link. The magnets exert a pulling force on the center links of each memory, holding the two memories together. The pulling force also results in additional friction between the two memories. It is thus important to use magnets that provide no more than the required force to hold the memories together.

Calculating the exact pulling force of permanent magnets is difficult and requires a finite element analysis. There are several online calculators that give an estimation of the pulling force of magnets in simple configurations. For example, a 3x3x1 N52 neodymium magnet located between two steel plates generates approximately 3N holding force [52]. The maximum gravitational force on each segment of the memory is significantly lower at approximately 0.015 N. Therefore, N52 neodymium magnets can provide sufficient force to hold the memories together. Finding the optimal magnet strength requires testing, which is done in the prototyping phase. To avoid other parts of the memories, such as the teeth and the side links, being affected by the magnets, they are manufactured from non-magnetic materials.

5.4 Control module

A control module has been designed to control locking, unlocking, and sliding of the memories. It contains three control levers. Two levers located at the rear side are called follower locks and control the follower memory (Figure 31a-d). One lever is located at the front, called the leader lock, and controls the leader memory (Figure 31d-f).

When all levers are pushed down, the mechanism is in its default configuration. Both memories will be locked, and the leader memory is one segment ahead of the follower memory. To obtain follow-the-leader locomotion from this default position, the following operating steps should be taken:

1. Move the leader lock up to unlock the leader memory.
2. Steer the leader segment manually to the desired direction.
3. Move the leader lock down to lock the leader memory.
4. Pinch the two follower locks together to unlock the follower memory.
5. Push the bottom follower lock up to unlock the follower memory.
6. Push the bottom follower lock further up to slide the follower memory to the top.
7. Hold the top follower lock in position while moving the bottom follower lock down to lock the follower memory.
8. Move the follower locks down while keeping them apart.

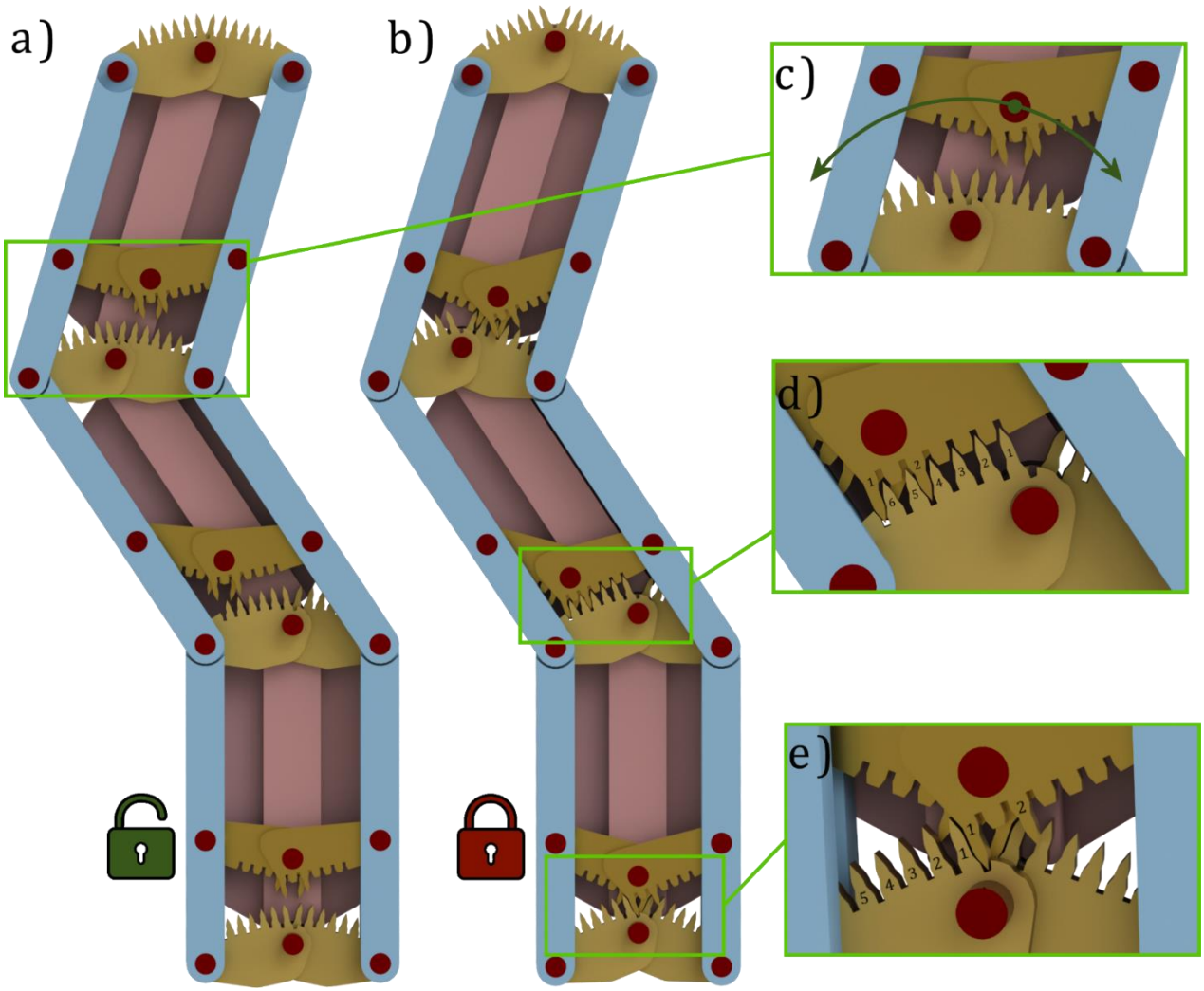

Figure 28: Illustration of three memory segments in unlocked and locked states, rendered in SolidWorks [55]. a) Memory in the unlocked state, each segment placed at an arbitrary angle. b) Memory in the locked state. c) Closeup of the unlocked locking mechanism, with its range of motion indicated. d) Closeup of the locked locking mechanism in the most extreme position. E) Closeup of the locked locking mechanism in the neutral position.

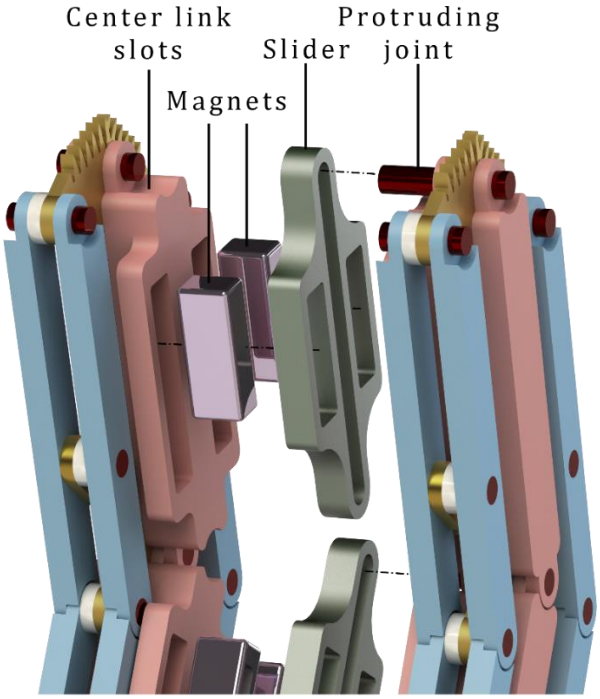

Figure 29: Exploded view sliding mechanism with its parts labelled. Render made in SolidWorks [55].

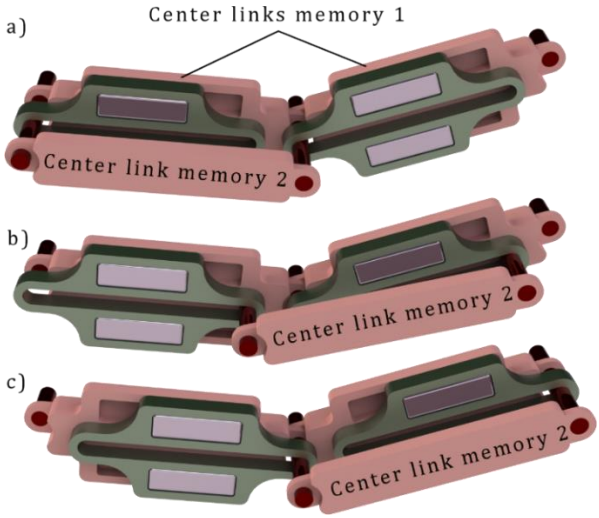

Figure 30: Illustration of the sliding mechanism's working principle. Only the sliders and center links of the two memories are shown for increased visibility. a) The center links of memory 1 and 2 are aligned. b) The center link of memory 2 is pushed to the right, its joint slides through the slot in the slider. c) The center link of memory 2 is pushed further, which causes the sliders to slide over the center links of memory 1. The center links of the memories are aligned again, shifted over one segment's length.

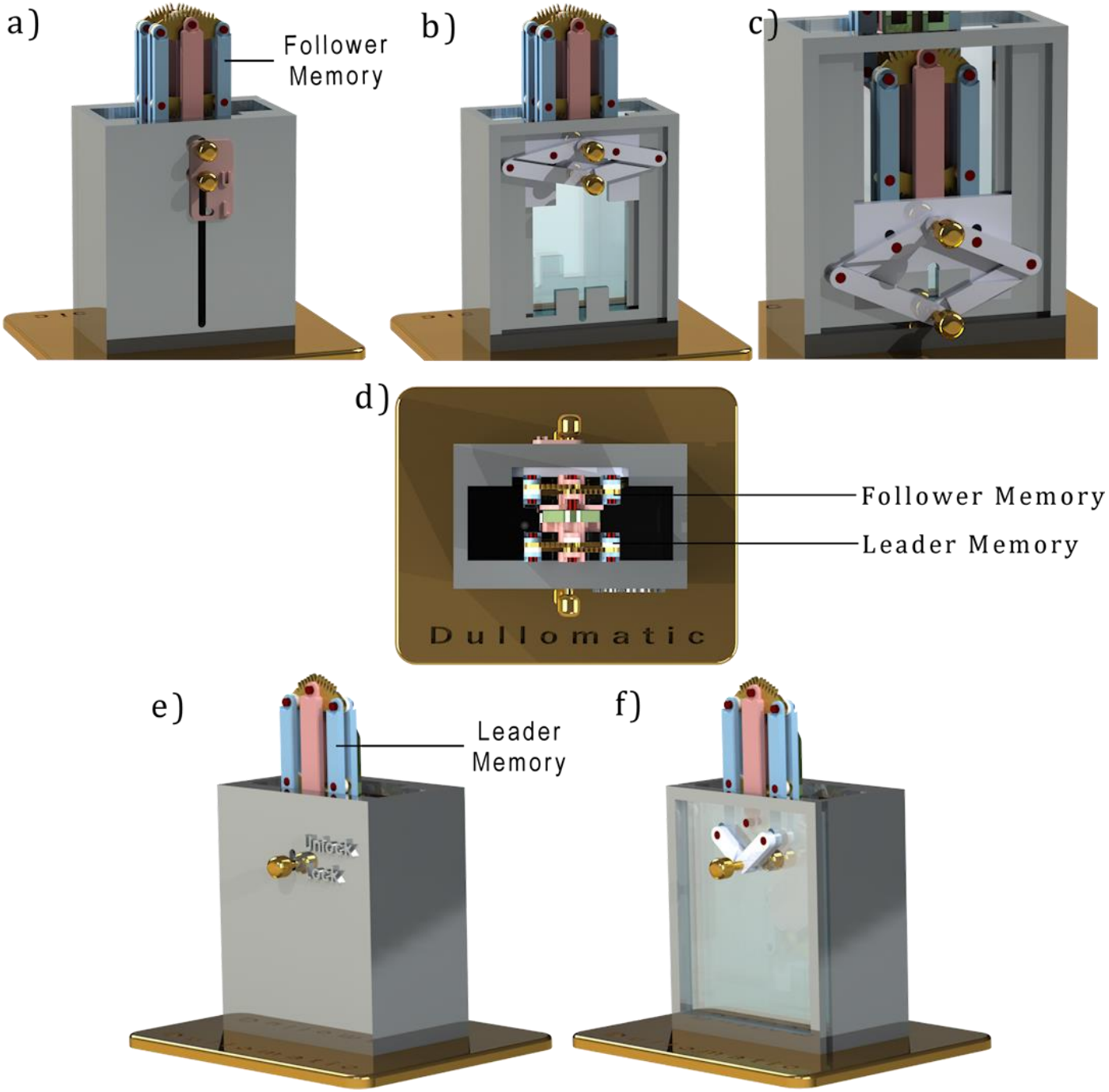

Figure 31: Overview of the control module. Renders made in SolidWorks. a) View of the back of the memory, showing the follower locks that control the follower memory. b) The mechanism behind the follower locks, containing a four-bar linkage mechanism connected to a sliding plate attached to the follower memory. The four-bar linkage mechanism is compressed, unlocking the follower memory. The sliding plate is at the top position, the follower memory aligned with the leader memory. c) The linkage mechanism is pulled apart, locking the follower memory. The sliding plate is at the bottom, the follower memory has slid down over one segment length. d) Top view of the control module, indicating the location of the follower memory and leader memory. e) Front view of the control module, showing the leader lock of the leader memory. f) A two-bar mechanism connects the leader lock to the memory.

The follower memory is attached to a slider inside the control module. This slider has a range of motion of 15 mm and can be moved by dragging the top follower lock up or down (Figure 31b-c). This causes the follower memory to slide up or down over the length of one segment with respect to the leader memory.

The follower memory can be locked or unlocked by changing the position of the bottom follower lock with respect to the top follower lock. When the bottom follower lock is pushed to the top follower lock, the follower memory is locked (Figure 31b). When the bottom follower lock is pushed away from the top follower lock, the follower memory is unlocked (Figure 31c).

A four-bar linkage mechanism connects the bottom follower lever to the follower memory (Figure 31b-c). The top joint is connected to the center link of the follower memory. The two top links are connected to the side links

of the follower memory by joints in the middle of each link. When the linkage mechanism is compressed (Figure 31b), the top links spread which pushes the side links of the follower memory outwards, unlocking the follower memory.

The front side has one lever that actuates locking/unlocking of the leader memory. A two-bar linkage mechanism connects the lever to the side links of the leader memory. Pushing the leader lock up will push the side links of the leader memory outwards, unlocking the leader memory.

This control module has not been built and tested yet.

6 Prototyping

6.1 The Dullomega

Overview

To evaluate the working principles of a single memory, a large-scale demonstration model called the Dullomega was manufactured through 3D-printing. Three segments of the memory were designed, 3D printed and assembled. The CAD design is displayed in Figure 32a, whereas the 3D printed prototype is displayed in Figure 32b.

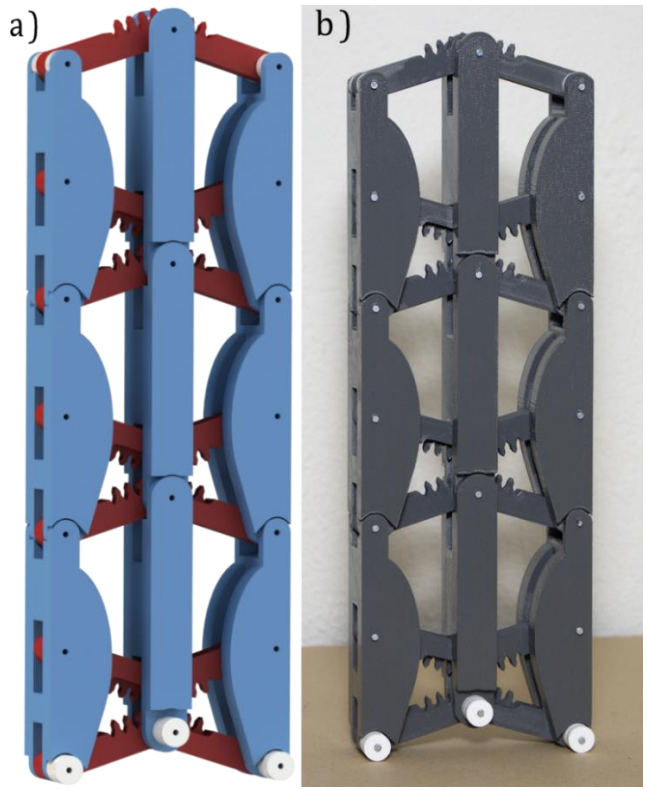

Figure 32: The Dullomega, a large-scale prototype containing three segments of one memory. a) Render of the Dullomega made in SolidWorks [51]. *b) 3D printed Dullomega.*

Manufacturing

Parts were manufactured on an Ultimaker 3 3D printer, using polyethylene terephthalate glycol (PETG). PETG has the benefit of being more durable than PLA which is more commonly used in FDM 3D printing. Two different printing profiles were used to decrease printing time. The center links and side links were printed at 70 mm/s and a layer height of 0.15mm, resulting in fast but less accurate prints. The segments with teeth were printed slower at 30mm/s and a layer height of 0.10 mm for increased accuracy.

Several attempts were made before the segments with teeth were printed successfully. The initial attempts resulted in teeth that would not fit into each other. Though PETG and PLA have quite similar printing characteristics, PETG requires slightly larger tolerances. Hence, the tolerances were increased to 0.3 mm. Secondly, inspection of the failed 3D prints showed that the first layer was larger than the rest of the print. This 3D printing issue is also known as elephant's foot [53], and was solved by slightly decreasing the material flow in the outer walls of the first layer to 95%.

Assembly

Standard nails (1.6 x 30 mm) were used to form the joints. A clearance fit was used to allow the nail to rotate freely to avoid unnecessary friction. 3D printed holes have a smaller diameter than in the respective CAD design, making it more difficult to find the correct hole diameter for a clearance fit. Through experimentation it was found that a 2 mm hole was adequate to achieve a close running fit. A transition fit was used between the nails and the teeth segments, so that only a moderate force would be required to drive the nails through the holes. The adequate hole size to achieve the transition fit was found experimentally to be 1.6 mm.

The joints of the center links and side links did not fit well into each other after 3D printing due to insufficient tolerances. This issue was increased by the slight warping of the joints due to heat build-up during 3D printing. A substantial amount of filing was done to make the joints fit.

6.2 Testing the Dullomega

The Dullomega was tested to determine whether the memory functions as well as in SolidWorks simulations. First, locking and unlocking of the memory was tested in a straight configuration, displayed in Figure 33a-b. The locking mode is engaged by bringing the outer control handles at the bottom segment closer to each other, resulting in the three segments locking simultaneously. Upon visual inspection the depth at which the teeth fall into each other is the same in all three segments. The amount of play in both the joints and teeth is negligible in this prototype. Once locked, the prototype was stiff.

Secondly, locking was tested with the mechanism in an arbitrary bent configuration, as displayed in Figure 33c-d. Close-ups of the locking mechanism are shown in

Figure 34. The mechanism worked as intended, being able to lock and unlock completely.

A downside of this prototype is the amount of force required to activate locking. When the pairs of teeth of each segment are perfectly aligned, locking requires minimal force as the teeth can slide easily into each other. However, when the teeth of a single segment are not aligned well, considerable force is required to slide the teeth into each other. When the misaligned teeth slide into each other, a clicking sound can be heard. This problem is likely exacerbated by the combination of the rough surface of the teeth and the stiffness of the joints. It does highlight that this could pose a problem in designs with a large number of segments, as misaligned teeth in a handful of segments could potentially block the entire mechanism from locking.

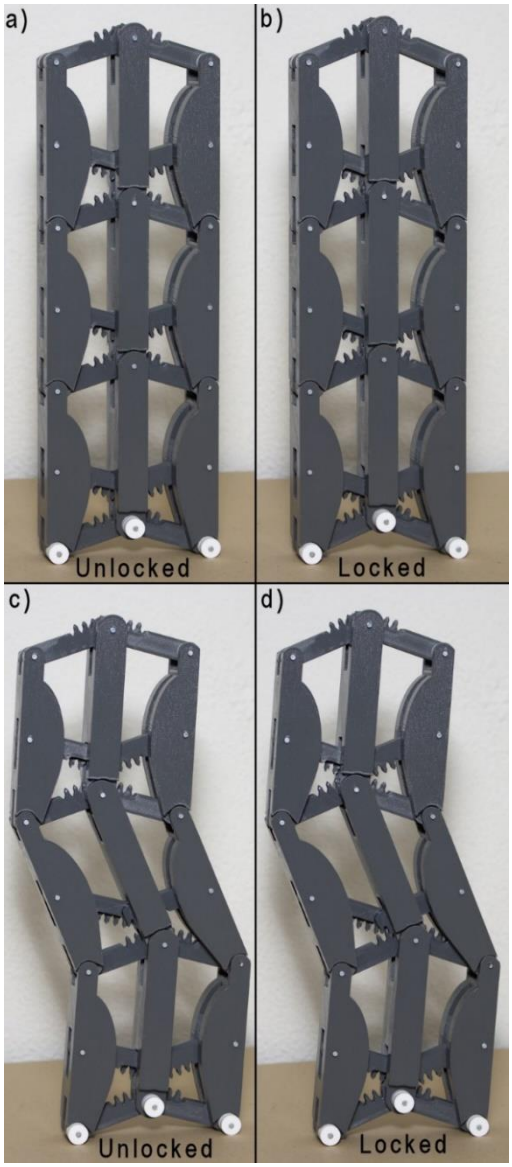

Figure 33: a) The Dullomega in an unlocked position, allowing segments to shear freely. b) The Dullomega in locked position, turning the mechanism in a stiff shaft. c) The Dullomega unlocked in an arbitrary position. d) The Dullomega locked in an arbitrary position.

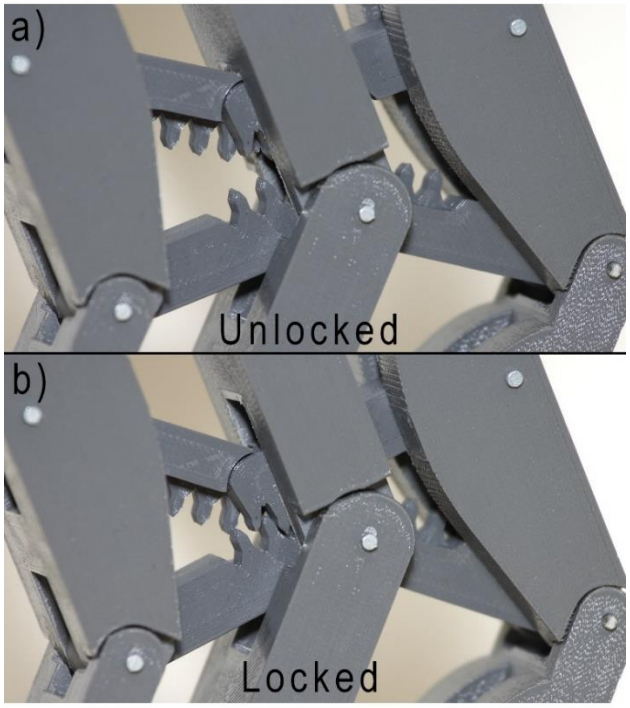

Figure 34: Close-ups of the locking mechanism of the Dullomini. a) The mechanism in unlocked position. b) The mechanism in locked position.

6.3 The Dullomini

Overview

The second prototype, called the Dullomini, contains two memories with three segments each, and is based on the final design. Originally it was planned to manufacture this prototype on a 1:1 scale. All parts could be manufactured by DEMO, but due to the large number of parts it would require too much time. Hence, 3D printing was looked at as an alternative. Using a Formlabs Form 3B SLA printer, it was found that parts at 1:1 scale could be printed accurately, but they would lack stiffness and break easily. However, at a 2:1 scale a sizeable portion of the parts could be printed with adequate stiffness. Therefore, it was decided to manufacture this prototype on a 2:1 scale, allowing a portion of the parts to be 3D printed while DEMO manufactured the teethed parts and metal parts.

Manufacturing

The design contains a large number of joints, which were made with dowel pins. The dowel pins have a diameter of 2 mm and two different lengths: 6 mm and 9.4 mm. Dowel pins with a length of 6 mm were available online, whereas dowel pins with a length of 9.4 mm were cut down from 10 mm on an EDM machine. Multiple standards for dowel pins exist. For this prototype, dowel pins according to DIN 6325 were used. The length of these dowel pins includes their rounded ends.

The links were printed on a Formlabs Form 3B with the resin Clear V4. This material provides a combination of high stiffness and high accuracy and can be printed with a layer thickness of 0.025 mm to obtain fine details.

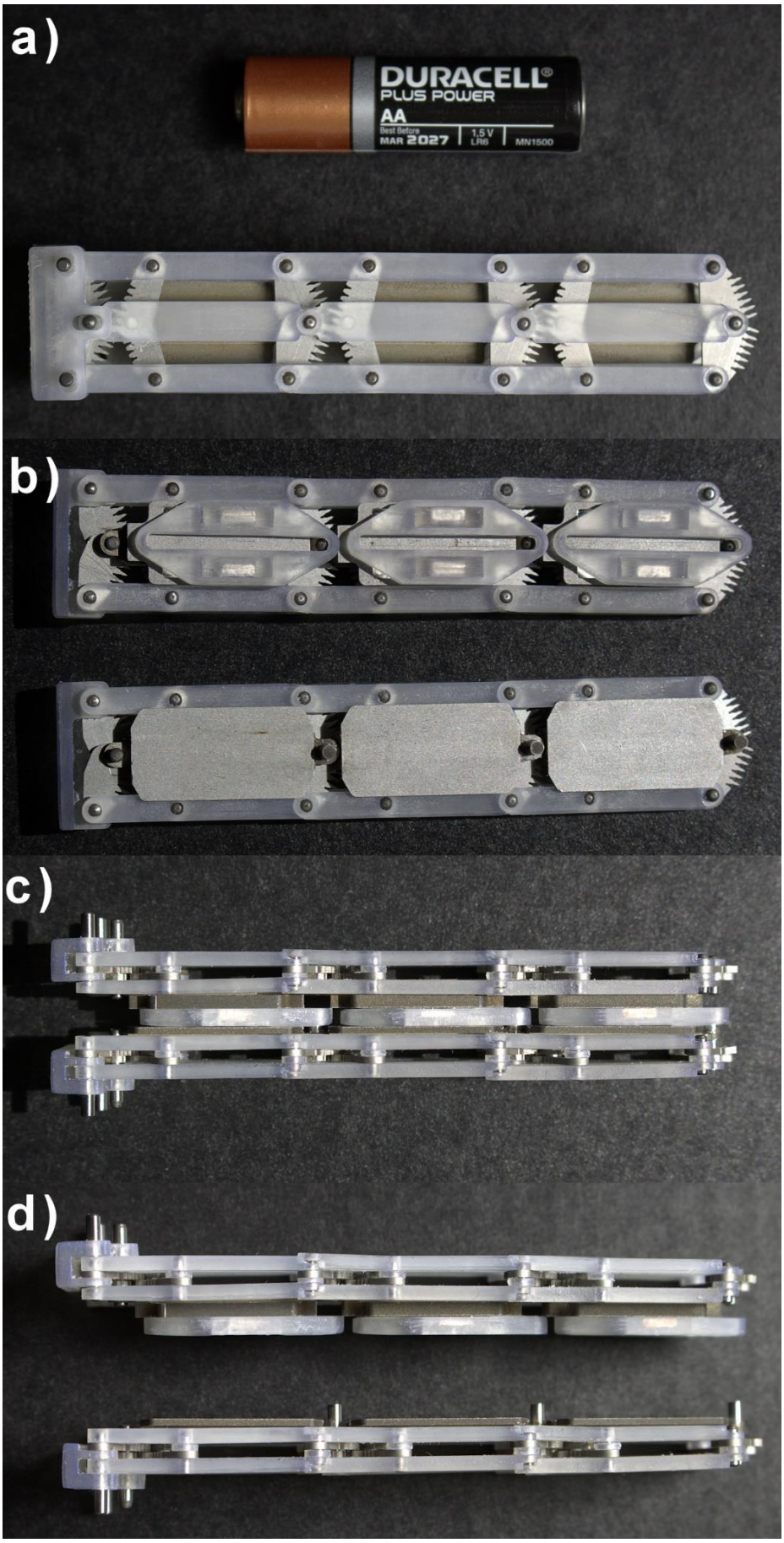

Figure 35:Photographs of the second prototype: the Dullomini. a) Top view of the Dullomini next to a standard AA battery to emphasise its small scale. b) Two halves of the Dullomini, displaying the sliding mechanism. c) Side view of the Dullomini. d) Side view of the Dullomini with the memories separated from each other.

Resins with better mechanical properties do exist, such as the Formlabs Tough series, meant for stiff and sturdy prototypes. However, those resins cannot be printed with a 0.025 mm layer thickness and hence the achievable accuracy is significantly lower.

Two types of fits are required to make the joints, clearance fits and interference fits. Holes in 3D printer parts tend to be smaller than intended. To obtain hole diameters corresponding to clearance and interference fits, a small block was 3D printed containing holes with diameters ranging from 2.00 mm to 2.20 mm with 0.02 mm increments. By pressing dowel pins into these holes, it was found that 2.06 mm holes were sufficient for an interference fit, and 2.12 mm holes for a clearance fit.

The segments were positioned with their thin side towards the build plate to reduce the required number of supports. The parts were then rotated 10 degrees over their longitudinal axis as recommended by Formlabs to increase the chance of a successful print. The support density was reduced to 75%, lowering the total number of supports and avoiding support placement at the holes. After printing, a metal wire was used to remove liquid resin from the holes of the uncured parts. Next, the parts were washed for 10 minutes in the Form Wash containing isopropyl alcohol, which dissolves liquid resin. Then, the uncured parts were carefully removed from the support structure and were cured over a couple of days in natural light. After curing, the surfaces where the supports had been were filed and then rinsed with water to obtain smooth and clean surfaces.

Assembly

The memories were assembled in three layers. The first layer consisted of the center links and side links of one side of the memory, which were connected by dowel pins. The side links contain two interference fits and one clearance fit. Pressing the dowel pins into the interference fit at the end of the part caused over half of the parts to break, making this step time consuming. The second layer consisted of the teethed parts and rings. These all have clearance fits, so they were placed rapidly. The third layer consisted of the side links and center links. The side links were 3D-printed again, but the interference fit that often broke during the assembly of the first layer was replaced by a clearance fit. This was effective, as no parts broke when assembling the third layer. Lastly, the magnets were placed into the sliders, and the sliders placed on the center links. The two memories were then connected by placing the extruding pins of one memory into the slots of the sliders of the other memory. The total assembly time was 12 hours.

Neodymium magnets are the strongest type of permanent magnet, and their strength is indicated by the letter N followed by a numerical value, ranging from 35 to 55. Their strength scales roughly linear with the grade. Although initially both N55 and N35 magnets were ordered, only N55 magnets could be delivered. It was found that N55 magnets with the design dimensions (10x4x3 mm) were too strong for this prototype and caused too much friction. Therefore, several smaller N55 block magnets were ordered and placed inside 3D printed blocks that matched the design dimensions. It was found that N55 block magnets (5x2x2 mm) inside a 3D printed block provided sufficient holding force while keeping friction forces acceptable.

6.4 Testing the Dullomini

Overview

The main functions of this prototype have been tested. First, the ability of the individual memories to lock in every position was tested. Secondly, a test was conducted to verify that the mechanism conserves the shape during propagation.

Locking positions

Each segment can be locked in a straight position (position 0), and six angled positions (positions 1-6) in two directions. The angle of the tip segment in each locked position in one direction is measured using a triangular ruler with markings on each degree. This is illustrated in Figure 36. The measured angles are reported in Table 2, as well as the respective angles of the CAD model. The mean absolute error between measured locking angle and modelled locking angle is 0.5 degrees.

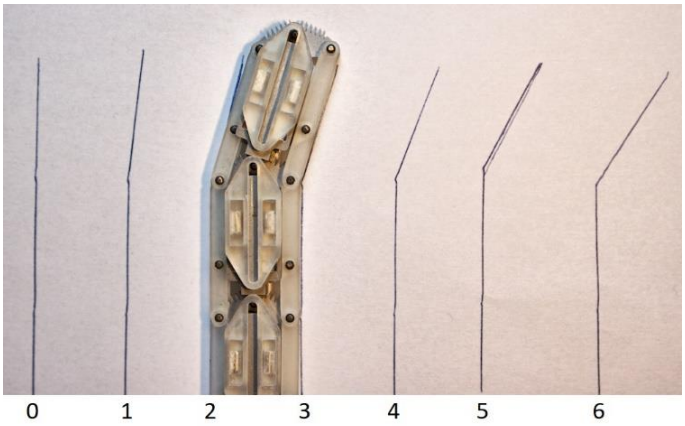

Figure 36: The contour of the memory in each locked position is outlined using a pen. The angle of the lines was measured using a triangular ruler to obtain the angles of the memory in each locked position.

Conservation of shape

An experiment was conducted to test whether the prototype can conserve its shape over multiple steps. A path was printed on a paper sheet, starting with three straight sections followed by four different angled curves (17°, 22°, -11°, -28°) congruent with the locking positions, spaced 30 mm (one segment length) away from each other. Next, the Dullomini was placed on the straight

Table 2: Measured angles, modelled angles, and absolute error of the tip segment

Locking Position	Measured Angle	Modelled Angle	Abs. Error
0	0°	0°	0°
1	6°	5.9°	0.1°
2	11°	11.5°	0.5°
3	17.5°	17°	0.5°
4	21.5°	22.4°	0.9°
5	28.5°	27.7°	0.8°
6	34°	33.3°	0.7°

sections and actuated through four propagation cycles to follow the curved path. In each step, the leader was manually steered to match the angle of the path section. The prototype was picked up from the sheet between the steps to actuate the mechanism. The first step indicating the complete propagation cycle is displayed in Figure 37. The starting and ending position at each step are displayed in Figure 38.

Photographs were taken at each step with a high resolution DSLR and enlarged to determine the locking position of each segment after each step. These locking positions are reported in Table 3.

Table 3: Locking positions of the segments at the end of each step. Positive positions are upwards, negative positions downwards.

	Locking position segment 1 (Leader)	Locking position segment 2 (Follower)	Locking position segment 3 (Follower)
Start	0	0	0
Step 1	3	0	0
Step 2	4	3	0
Step 3	-2	4	3
Step 4	-5	-2	4

7 Discussion

7.1 Evaluation

Two tests were conducted on a small-scale prototype of the Dullomatic. The angle of each shaft segment can be locked in 13 different positions with a maximum angle of 34 degrees, allowing the shaft to follow a wide range of paths. The shape conservation test demonstrates that each locked position shifts backwards through the instrument as the instrument moves forward. These results suggest that Dullomatic is able to propagate with FTL locomotion over 2D paths. The shape conservation mechanism can be actuated by forces applied through the base of the instrument, hence the instrument is likely able to conserve shape in areas of the body where contact between the instrument and tissue surrounding the path has to be avoided.

The tests conducted on the prototype have several limitations. First of all, a limited number of tests could be conducted because the 3D printed parts of the prototype are vulnerable. These parts are to be replaced with metal parts to allow for more rigorous testing. The stiffness of the design must also be tested once a sturdier prototype has been manufactured. Secondly, the prototype contains only three segments and can therefore only assume a limited number of shapes. Also, the effect of play is small with few segments but could play a larger role in a prototype with more segments. State-of-the-art devices frequently suffer from shape damping [17][31][47][48]. This effect was not observed during the testing of this prototype. A new prototype containing at least 5 segments should be built to test the Dullomatic's ability to follow S curves and to verify that the shape is not damped in this design.

Manual assembly of the shaft containing 3 segments took 12 hours. The assembly time can be drastically reduced by using custom assembly tools and an assembly robot. The memories can be assembled by placing the parts in a fixture that holds each part in the correct location. All joints have the same orientation, and hence all dowel pins can be pressed in simultaneously by a large press.

Improvements

The Dullomatic can be improved by reducing its diameter. The current prototype was manufactured at a 2:1 scale because smaller parts would take too long to manufacture. However, all parts are manufacturable at their original size, which would result in a 10 mm wide instrument. The diameter can be reduced even further. The parts were designed to be manufacturable on a standard EDM machine using a 0.1 mm wire. There are EDM machines that use wires of 0.02 mm [54], allowing the parts to be manufactured 4 to 5 times smaller, resulting in an instrument between 2.5 mm and 2 mm in diameter. It should be noted that manufacturing and assembly would become considerably more difficult, time-consuming and expensive. There would also be scalability issues, such as parts having insufficient stiffness and friction becoming more pronounced.

The memory segments contain 13 distinct locking positions, however, these current positions are arbitrary. If some information about the path to be taken in the body is already known, the position and number of locking teeth can be customised to that path. By strategically choosing fewer, but better positioned

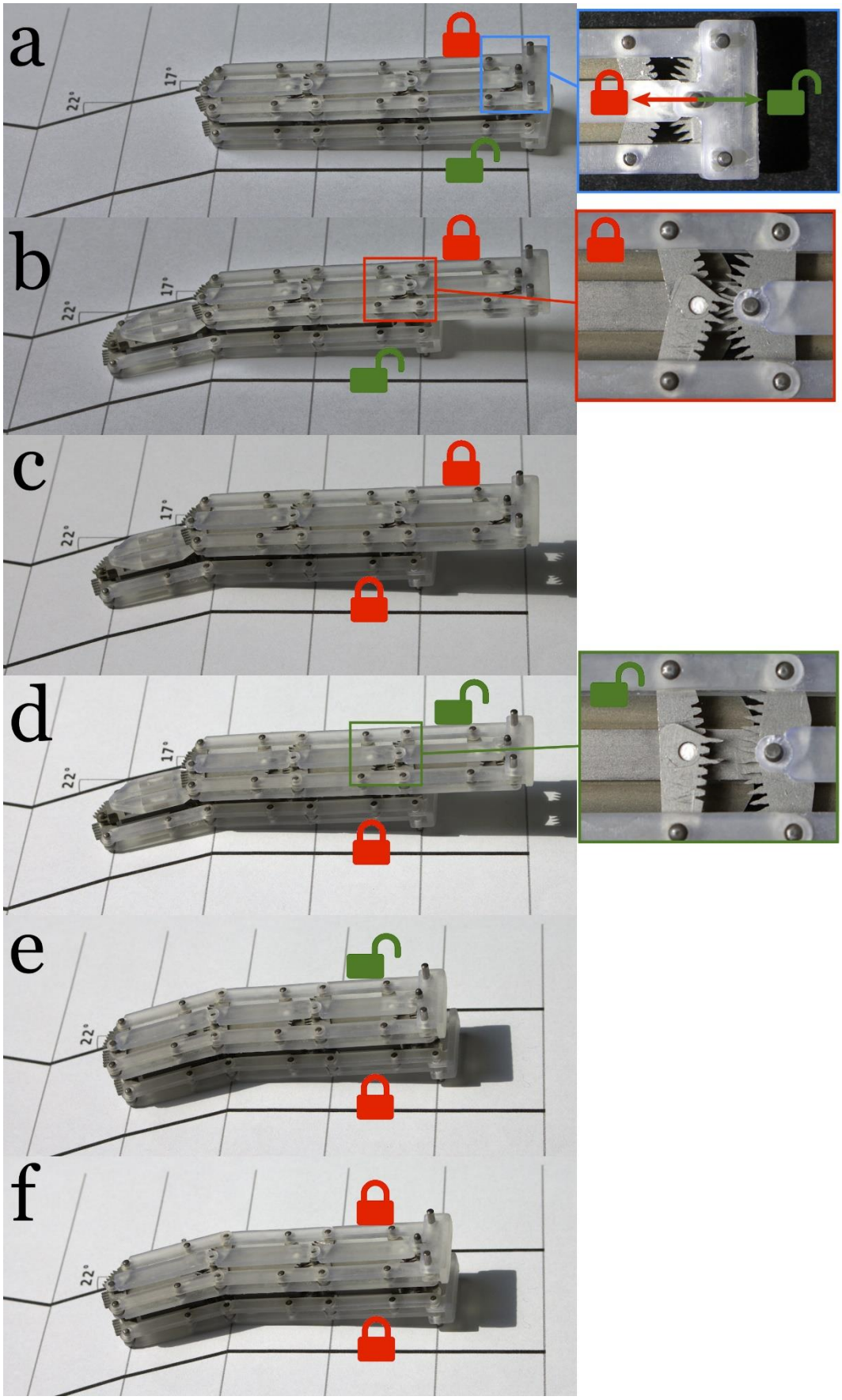

Figure 37: Photographs of the Dullomini during a forward propagation step. a) The follower memory is locked, the leader memory unlocked. Locking of each memory is controlled by pushing the protruding pin at middle of the base forward to lock and backward to unlock. b) The leader memory has been slid forward and manually steered to match the angle of the path. c) The leader memory is locked. d) The follower memory is unlocked. e) The follower memory is slid forward to copy the shape of the leader memory. f) The follower memory is locked and now holds the shape of the leader memory.

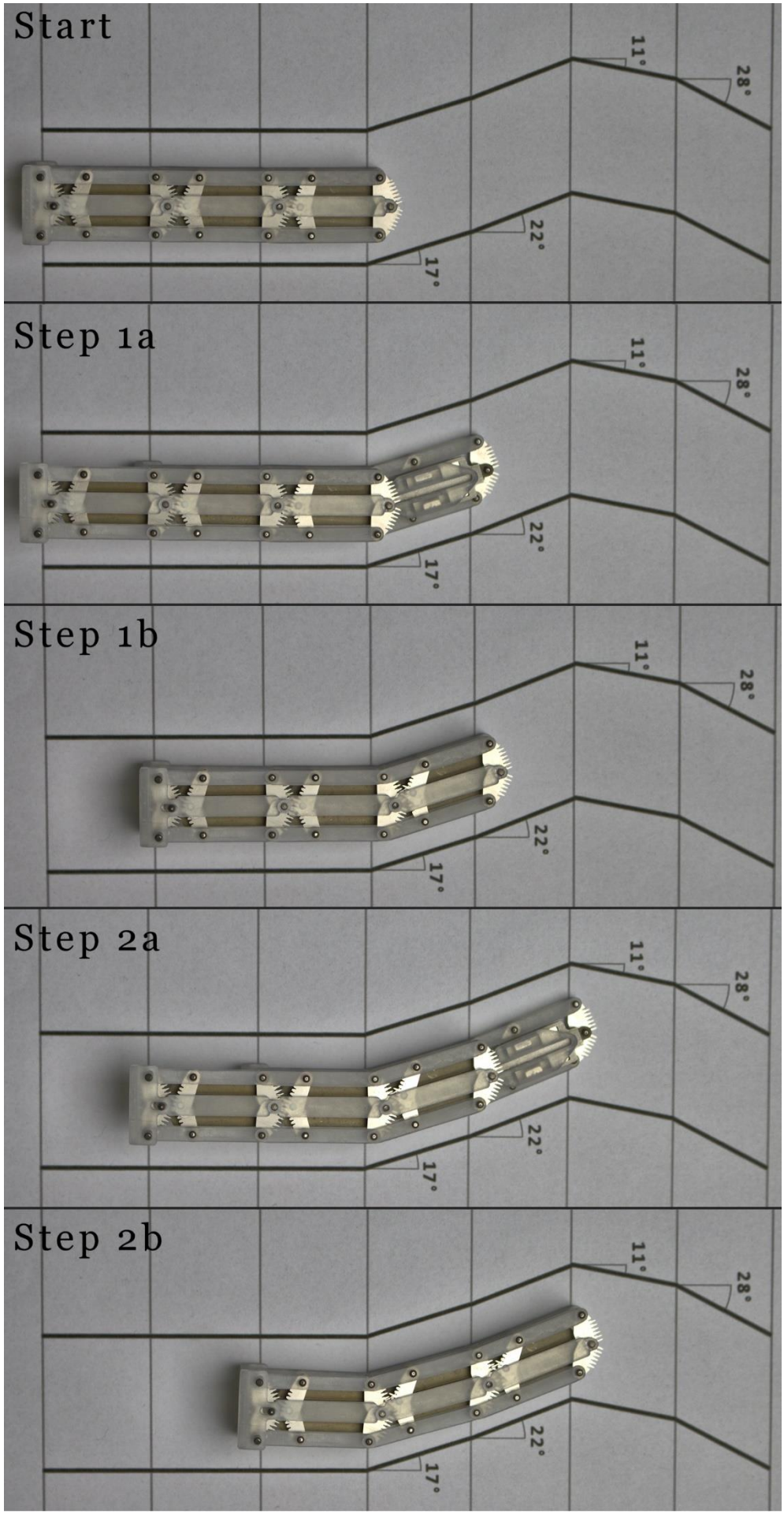

Figure continues on the next page.

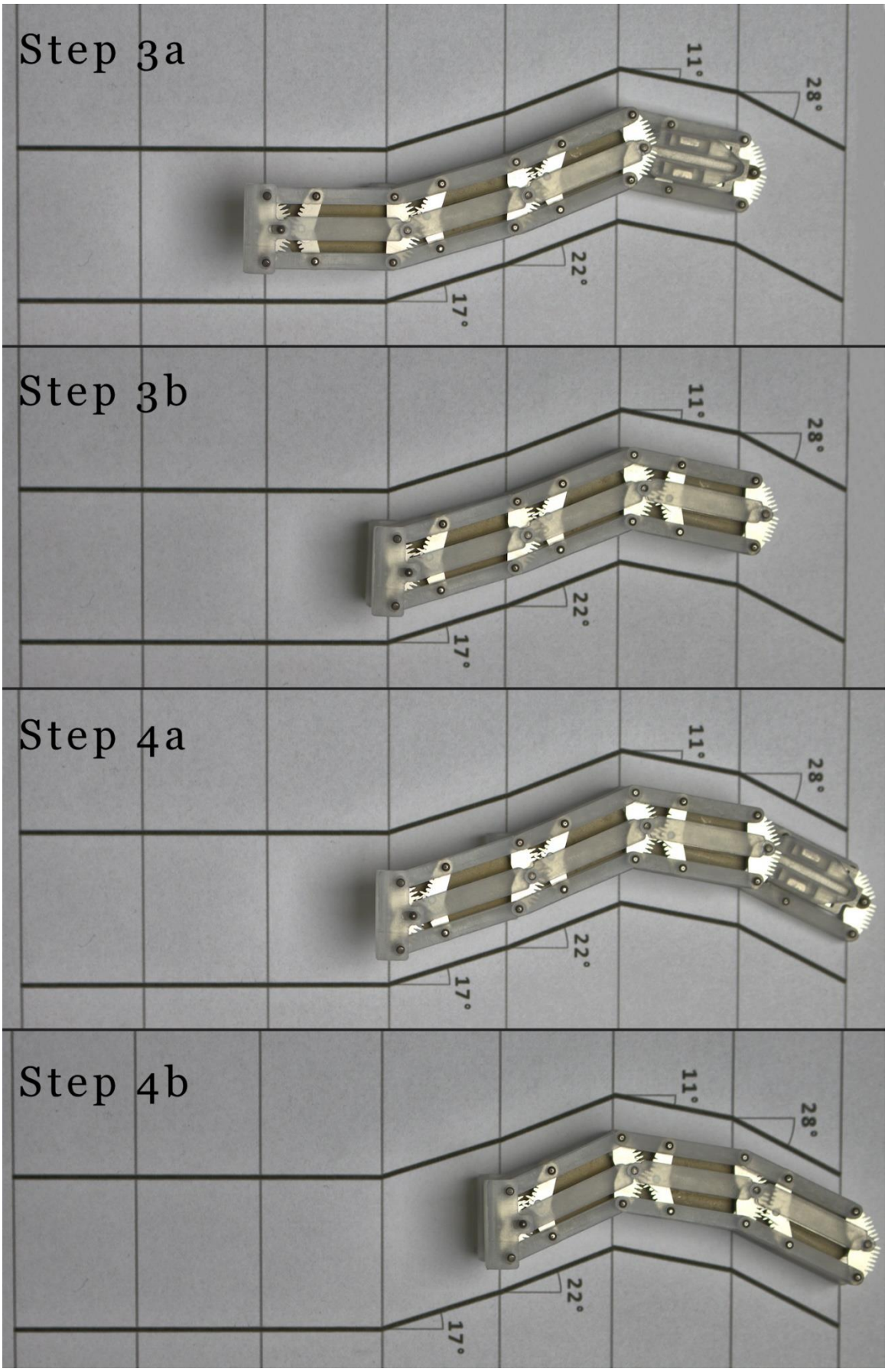

Figure 38: Shape conservation test of the Dullomini. The prototype propagates through a curved trajectory containing four different angles. The angles of the segments were measured at the end of each step and are reported in Table 3.

locking teeth, their size can be increased, potentially augmenting the locked stiffness of the device while also allowing for simpler manufacturing.

The use of magnets to keep the memories together is ideal for prototyping because it simplifies assembly. However, use of magnets inside surgical tools is generally undesirable as magnetic fields can affect pacemakers [55] and they cannot be used in conjunction with MRI scans. Furthermore, the magnetic force contributes significantly to the friction between the memories. Therefore, different methods to hold the memories together should be explored. One possibility is to use rivet-like fasteners, as illustrated in Figure 39.

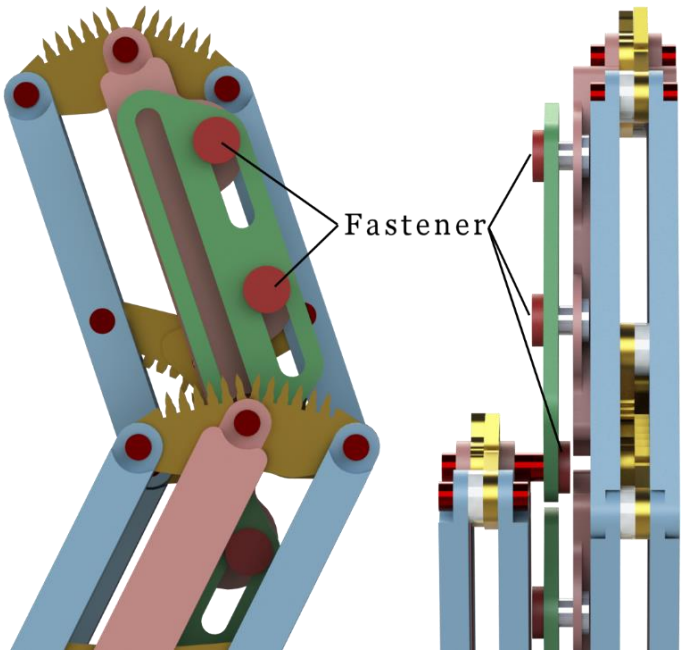

Figure 39: The magnets between the memories can be replaced by fasteners to reduce friction.

7.2 Design limitations

The Dullomatic does have downsides compared to state-of-the-art devices. Primarily, it can only follow paths in 2D and can therefore not be used in surgeries that require the instrument to follow a 3D path, such as in colonoscopy. Secondly, the instrument has relatively large outer dimensions, making it too large for some natural orifices such as the nose in endonasal surgery [56]. Thirdly, the range of motion of the instrument is too small for some forms of minimally invasive surgery, such as endoscopy. The Dullomatic cannot make the large bend required to enter the sigmoid colon from the rectum. However, its precise positioning ability and high locked stiffness suggest it may find application in cases where clinicians need to exert a large amount of force on the body, such as in tissue stabilisation.

Exploring a 3D Dullomatic

A conceptual 3D memory containing the same locking method as the Dullomatic is displayed in Figure 40. Many new challenges arise when designing a 3D version of the Dullomatic. First, the upper jaw moves in 3D as the segment shears to a new position. However, the center link forms an obstacle in the path of the upper jaw, severely limiting the range of motion of the upper jaw and thus the segment. Secondly, the lower jaw must have locking positions distributed over a cone-shaped surface area. One option is to design a compliant cone-shaped lower jaw. This lower jaw would be deformed during locking making its design difficult. Thirdly, connecting two 3D shape memories to each other is exceedingly difficult. The slider mechanism used in the Dullomatic will not work on a 3D shape memory as it requires a flat plane to slide over.

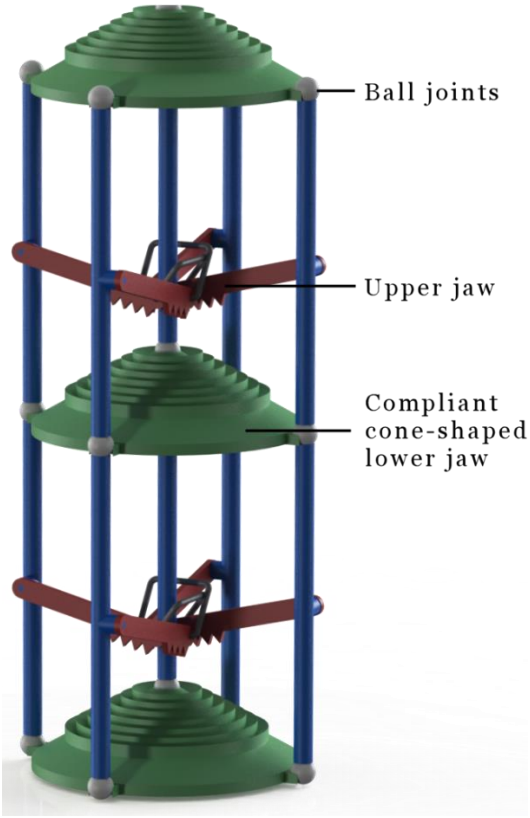

Figure 40: Concept of a 3D shape memory based on the locking method of the Dullomatic.

It is therefore questionable whether the Dullomatic's mechanisms should form a foundation for a 3D shape memory, as it becomes an exceedingly complex mechanism. Even if all challenges were solved, the resulting mechanism would likely be much larger than the Dullomatic, and likely too large for its purpose. Instead, the Dullomatic has more potential to be used in a guiding instrument for a cable-actuated 3D FTL device that propagates from the Dullomatic's tip. This could be useful when the first part of the anatomical pathway is 2D and the last part is 3D.

7.3 Potential future use cases

One potential future use case for the Dullomatic is in assisting bronchoscopy. During this procedure, the patient lies with their head tilted upwards to allow a tool to pass from the mouth or nose into the lungs. This is displayed in Figure 41. The path from the mouth down to the bottom of the trachea where it branches into the bronchi can be considered 2D and has a diameter between 10 mm and 27 mm in adults [57]. The Dullomatic might be used to form a stiff guiding tool to reach the bottom of the trachea, where thinner tools can propagate from the Dullomatic into the bronchi.

Another potential future use for the Dullomatic is in minimally invasive surgery on large endangered species such as elephants and rhinoceroses. These animals are much larger than humans and have larger natural orifices, therefore larger surgical instruments could be used. Traditional abdominal surgery on these animals has had limited success, while laparoscopic surgery has been performed with success [58]. The flexibility of the Dullomatic can simplify manoeuvring through the abdominal region of these animals.

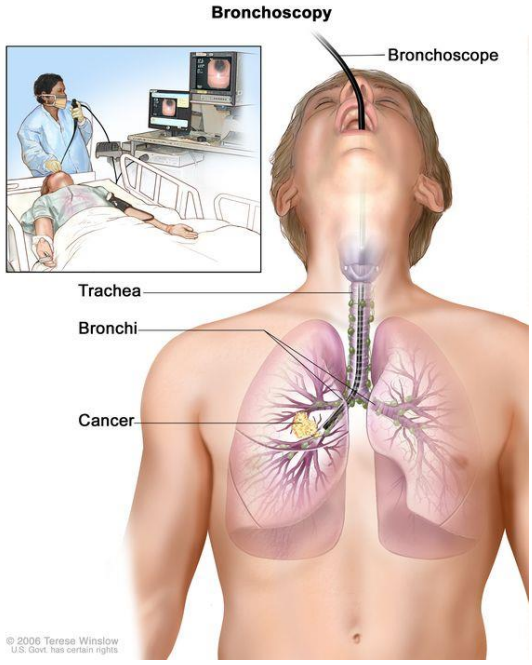

Figure 41: Illustration of a bronchoscopic procedure. The patient's head is tilted back, resulting in a straighter path from the oral cavity to the trachea. Image derived from [59].

7.4 Future work

A steering mechanism should be added to steer the leader. One idea is to attach steering cables to the leader, as displayed in Figure 42. The pair of cables run parallel to the side links of the follower segments and connect to the center link of the leader segment. By pulling one cable and releasing the other cable, the leader can be steered. Additional parts are needed to hold these steering cables in place. It should be explored whether these steering cables can run on the inside of the memory without becoming entangled in any teethed elements. The steering cables could also run on the outside of the memory, but that would increase the thickness of the shaft and is therefore a less preferable option.

The current control module contains three levers to control the individual functions of the shaft: locking each memory and shifting the memories. This is ideal for testing purposes, as each individual function can be tested. This does increase the difficulty of controlling the shaft. The control sequence is always the same, hence a new control module could be designed that has only one crank that actuates all three functions in the correct sequence.

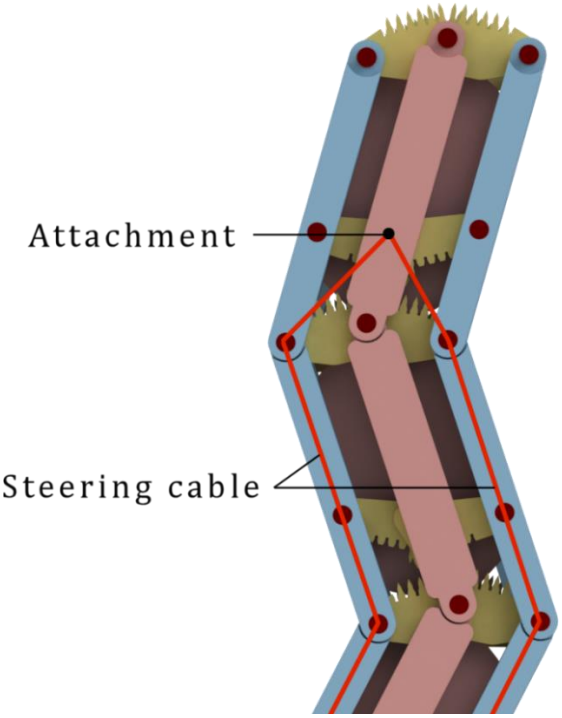

Figure 42: Steering concept. A pair of antagonistic steering cables are attached to the leaders center link and run down past the side links to the control unit. Pulling one cable while releasing the other cable will steer the leader.

The shaft moves forward during every propagation step, which can be realized by mounting the control module on a rail system. An impression of this concept is displayed in Figure 43. Rotating the blue crank causes the control module to move forward/backwards and actuates propagation or retraction of the shaft. One full rotation of the blue crank corresponds to one propagation step. The leader can be steered by rotating the red crank. The angle of the red crank corresponds to the angle of the leader, simplifying the shaft's control.

The shaft should be covered by a protective sleeve to keep tissue from entering the mechanism. The teeth inside the memories have sharp tips that could otherwise puncture tissue. The sleeve should be made from elastic and biocompatible material, such as silicone. Care should be taken that this sleeve does not enter the memories itself either, as that could cause jamming.

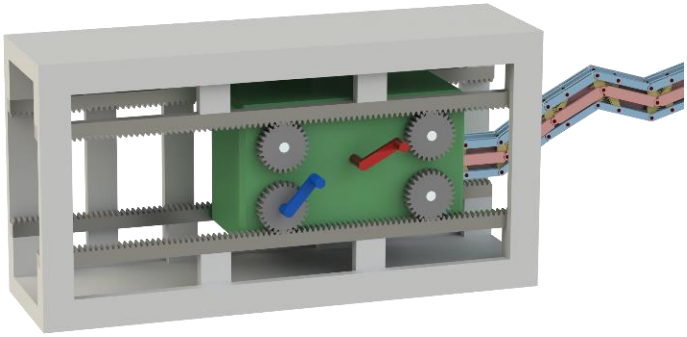

Figure 43: Impression of the control unit (green) mounted on a track. By rotating the blue crank, the control unit and shaft moves forward or backwards. This also actuates the shape sliding mechanism of the shaft. The red crank is used to steer the leader.

7.5 Outlook

The test results suggest that the Dullomatic can follow 2D paths. It has done so accurately and without the shaft's shape being damped or lost, which is an advantage over various state of the art designs. However, its potential use cases are limited to anatomical pathways and surgical methods where the shape of the path falls in one plane. Albeit the Dullomatic has less use cases than an instrument that can follow a 3D path, it does offer more manoeuvrability than conventional rigid instruments. The Dullomatic seems relatively stiff and could potentially be used as a guiding tool for various surgical tools. The Dullomatic therefore forms an interesting addition to the field of FTL instruments.

8 Conclusion

In the future, minimally invasive surgery (MIS) could benefit from flexible follow-the-leader (FTL) instruments, which are envisaged to move with snake-like locomotion to get to areas in the human body that are difficult to reach with rigid instruments. A challenging design aspect of FTL instruments is to conserve the instrument's shape accurately while the instrument propagates into or retracts from the body. An interesting novel approach are so called mechanical shape memories, which remain outside of the body and control the shape of a thin flexible shaft through cables. However, these cables stretch under tension, causing damping of the instrument's shape.

In this research a mechanical shape memory that fits inside a flexible shaft was designed, prototyped, tested and evaluated. Three concepts were proposed and compared, one of which formed the basis of the final design. This final design, called the Dullomatic, contains two shape memory mechanisms which can slide over each other to shift the instrument's shape backwards as the instrument propagates forward. A single shape memory was first prototyped at a 9:1 scale to verify the concept works as intended. Next, a 2:1 scale prototype of the Dullomatic containing three segments was manufactured. Test results of the 2:1 scale prototype suggests that the Dullomatic can conserve a 2D shape accurately and without shape damping. The prototype can be manually operated to obtain follow-the-leader locomotion. Additional research is required to develop a control unit and incorporate a steering mechanism into the Dullomatic.

The Dullomatic is an interesting design, and its test results suggest that it could be used to manoeuvre through 2D paths with FTL locomotion. It forms a good addition to the field of FTL instruments and could potentially aid in further reducing the invasiveness of surgery.

9 Bibliography

[1] B. Jaffray, “Minimally invasive surgery,” *Arch. Dis. Child.*, vol. 90, no. 5, pp. 537–542, May 2005, doi: 10.1136/ADC.2004.062760.

[2] H. Australia, “Laparoscopy,” 2022, Accessed: Oct. 18, 2022. [Online]. Available: https://www.healthdirect.gov.au/laparoscopy.

[3] W. G. Mouton, J. R. Bessell, K. T. Otten, and G. J. Maddern, “Pain after laparoscopy,” *Surg. Endosc. 1999 135*, vol. 13, no. 5, pp. 445–448, Feb. 2014, doi: 10.1007/S004649901011.

[4] P. V. Theodosopoulos, B. Guthikonda, A. Brescia, J. T. Keller, and L. A. Zimmer, “Endoscopic Approach to the Infratemporal Fossa,” *Neurosurgery*, vol. 66, no. 1, pp. 196–203, Jan. 2010, doi: 10.1227/01.NEU.0000359224.75185.43.

[5] A. N. Kalloo, “Natural Orifice Transluminal Endoscopic Surgery (NOTES),” *Gastroenterol. Hepatol. (N. Y).*, vol. 3, no. 3, p. 183, Mar. 2007, Accessed: Oct. 11, 2022. [Online]. Available: /pmc/articles/PMC3099337/.

[6] B.-J. Yi and H.-S. Yoon, “Review of Computer-Aided Sinus Surgery,” *Hanyang Med. Rev.*, vol. 36, no. 4, p. 248, 2016, doi: 10.7599/HMR.2016.36.4.248.

[7] I. Sugarman and J. Sutcliffe, “Colonoscopy,” *Oper. Pediatr. Surg. Seventh Ed.*, pp. 104–111, Jul. 2022, doi: 10.1201/b13198-24.

[8] K. S. Spector and W. E. Lawson, “Optimizing safe femoral access during cardiac catheterization,” *Catheter. Cardiovasc. Interv.*, vol. 53, no. 2, pp. 209–212, Jun. 2001, doi: 10.1002/CCD.1150.

[9] S. Beniwal, K. Bhargava, and S. K. Kausik, “Size of distal radial and distal ulnar arteries in adults of southern Rajasthan and their implications for percutaneous coronary interventions,” *Indian Heart J.*, vol. 66, no. 5, p. 506, Sep. 2014, doi: 10.1016/J.IHJ.2014.08.010.

[10] L. Blanc, A. Delchambre, and P. Lambert, “Flexible Medical Devices: Review of Controllable Stiffness Solutions,” *Actuators 2017, Vol. 6, Page 23*, vol. 6, no. 3, p. 23, Jul. 2017, doi: 10.3390/ACT6030023.

[11] H. Choset and W. Henning, “A Follow-The-Leader Approach to Serpentine Robot Motion Planning,” vol. 12, no. April, pp. 65–73, 1999, [Online]. Available: https://ascelibrary.org/doi/pdf/10.1061/%28ASCE%290893-1321%281999%2912%3A2%2865%29.

[12] P. W. J. Henselmans, S. Gottenbos, G. Smit, and P. Breedveld, “The MemoSlide: An explorative study into a novel mechanical follow-the-leader mechanism,” *Proc. Inst. Mech. Eng. Part H J. Eng. Med.*, vol. 231, no. 12, pp. 1213–1223, Dec. 2017, doi: 10.1177/0954411917740388.

[13] Coronado National Memorial, “You never know who might stop by the visitor center. Yesterday this Sonoran mountain kingsnake (Lampropeltis pyromelana) showed off its climbing skills on our adobe walls. | Facebook,” 2022. https://www.facebook.com/watch/?v=856685765319018 (accessed Oct. 27, 2022).

[14] J. Burgner-Kahrs, D. C. Rucker, and H. Choset, “Continuum Robots for Medical Applications: A Survey,” *IEEE Trans. Robot.*, vol. 31, no. 6, pp. 1261–1280, Dec. 2015, doi: 10.1109/TRO.2015.2489500.

[15] C. Culmone, F. S. Yikilmaz, F. Trauzettel, and P. Breedveld, “Follow-The-Leader Mechanisms in Medical Devices: A Review on Scientific and Patent Literature,” *IEEE Rev. Biomed. Eng.*, vol. 16, pp. 439–455, 2023, doi: 10.1109/RBME.2021.3113395.

[16] P. W. J. Henselmans, G. Smit, and P. Breedveld, “Mechanical Follow-the-Leader motion of a hyper-redundant surgical instrument: Proof-of-concept prototype and first tests,” *Inst. Mech. Eng. Proceedings. Part H J. Eng. Med.*, vol. 233, no. 11, pp. 1141–1150, Nov. 2019, doi: 10.1177/0954411919876466.

[17] P. W. J. Henselmans, C. Culmone, D. J. Jager, R. I. B. van Starkenburg, and P. Breedveld, “The MemoFlex II, a non-robotic approach to follow-the-leader motion of a snake-like instrument for surgery using four predetermined physical tracks,” *Med. Eng. Phys.*, vol. 86, pp. 86–95, Dec. 2020, doi: 10.1016/j.medengphy.2020.10.013.

[18] F. Semih Yikilmaz, “Alternating Follow-the-Leader Medical Device with Pneumatically Actuated Shape Locks.” 2021, Accessed: Oct. 11, 2022. [Online]. Available: https://repository.tudelft.nl/islandora/object/uuid%3A99f2a1ee-d1da-4b9c-829a-ac80f05ed3e7.

[19] A. Degani, H. Choset, A. Wolf, and M. A. Zenati, “Highly Articulated Robotic Probe for Minimally Invasive Surgery,” *Conf. Proc. IEEE Eng. Med. Biol. Soc.*, vol. 2006, no. 1642343, p. 4167, 2006, doi: 10.1109/ROBOT.2006.1642343.

[20] H. M. Choset, A. Wolf, and M. A. Zenati, “US9011318B2 - Steerable, follow the leader device - Google Patents.” https://patents.google.com/patent/US9011318?oq=Steerable%2C+follow+the+leader+device. (accessed Nov. 09, 2022).

[21] C. Y. Chen *et al.*, “Multi-turn, tension-stiffening catheter navigation system,” *IEEE Int. Conf. Intell. Robot. Syst.*, 2010, doi: http://dx.doi.org/10.1109/ROBOT.2010.5509786.

[22] “Shape lockable apparatus and method for advancing an instrument through unsupported anatomy,” Jul. 2004.

[23] L. Dupourqué, F. Masaki, Y. L. Colson, T. Kato, and N. Hata, “Transbronchial biopsy catheter enhanced by a multisection continuum robot with follow-the-leader motion,” *Int. J. Comput. Assist. Radiol. Surg.*, vol. 14, no. 11, pp. 2021–2029, Nov. 2019, doi: 10.1007/S11548-019-02017-W/FIGURES/13.

[24] P. W. J. Henselmans, S. Gottenbos, G. Smit, and P. Breedveld, “The MemoSlide: An explorative study into a novel mechanical follow-the-leader mechanism,” *Proc. Inst. Mech. Eng. Part H J. Eng. Med.*, vol. 231, no. 12, pp. 1213–1223, Dec. 2017, doi: 10.1177/0954411917740388.

[25] K. Ikuta, M. Tsukamoto, and S. Hirose, “Shape Memory Alloy Servo Actuator System with Electric Resistance Feedback and Application for Active Endoscope,” pp. 427–430, 1988, doi: 10.1109/ROBOT.1988.12085.

[26] Y. Chen, J. Liang, and I. W. Hunter, “Modular continuum robotic endoscope design and path planning,” *Proc. - IEEE Int. Conf. Robot. Autom.*, pp. 5393–5400, 2014, doi: 10.1109/ICRA.2014.6907652.

[27] J. Son *et al.*, “A novel semi-automatic snake robot for natural orifice transluminal endoscopic surgery: preclinical tests in animal and human cadaver models (with video),” *Surg. Endosc.*, vol. 29, no. 6, pp. 1643–1647, Jun. 2015, doi: 10.1007/S00464-014-3854-6/FIGURES/3.

[28] R. O. Buckingham and A. C. Graham, “Computer controlled redundant endoscopy,” *Proc. IEEE Int. Conf. Syst. Man Cybern.*, vol. 3, pp. 1779–1783, 1996, doi: 10.1109/ICSMC.1996.565377.

[29] “FAULHABER B-Micro 0308 ... B.” https://www.faulhaber.com/en/products/series/0308b/ (accessed Oct. 07, 2022).

[30] Y. Chen, J. Liang, and I. W. Hunter, “Modular continuum robotic endoscope design and path planning,” *undefined*, pp. 5393–5400, Sep. 2014, doi: 10.1109/ICRA.2014.6907652.

[31] Y. Gao, K. Takagi, T. Kato, N. Shono, and N. Hata, “Continuum Robot with Follow-the-Leader Motion for Endoscopic Third Ventriculostomy and Tumor Biopsy,” *IEEE Trans. Biomed. Eng.*, vol. 67, no. 2, p. 379, Feb. 2020, doi: 10.1109/TBME.2019.2913752.

[32] A. Arora, Y. Ambe, T. H. Kim, R. Ariizumi, and F. Matsuno, “Development of a maneuverable flexible manipulator for minimally invasive surgery with varied stiffness,” *Artif. Life Robot.*, vol. 19, no. 4, pp. 340–346, Dec. 2014, doi: 10.1007/S10015-014-0184-7/TABLES/1.

[33] S. Tappe, J. Pohlmann, J. Kotlarski, and T. Ortmaier, “Towards a follow-the-leader control for a binary actuated hyper-redundant manipulator,” *IEEE Int. Conf. Intell. Robot. Syst.*, vol. 2015-December, pp. 3195–3201, Dec. 2015, doi: 10.1109/IROS.2015.7353820.

[34] S. Tappe, J. Kotlarski, T. Ortmaier, M. Dorbaum, A. Mertens, and B. Ponick, “The kinematic synthesis of a spatial, hyper-redundant system based on binary electromagnetic actuators,” in *2015 6th International Conference on Automation, Robotics and Applications (ICARA)*, Feb. 2015, pp. 211–216, doi: 10.1109/ICARA.2015.7081149.

[35] F. Campisano *et al.*, “Closed-loop control of soft continuum manipulators under tip follower actuation,” *Int. J. Rob. Res.*, vol. 40, no. 6–7, pp. 923–938, Jun. 2021, doi: 10.1177/0278364921997167/ASSET/IMAGES/LARGE/10.1177_0278364921997167-FIG2.JPEG.

[36] H. B. Gilbert and R. J. Webster, “Can concentric tube robots follow the leader?,” in *Proceedings - IEEE International Conference on Robotics and Automation*, 2013, pp. 4881–4887, doi: 10.1109/ICRA.2013.6631274.

[37] E. Amanov, J. Granna, and J. Burgner-Kahrs, “Toward improving path following motion: Hybrid continuum robot design,” *Proc. - IEEE Int. Conf. Robot. Autom.*, pp. 4666–4672, Jul. 2017, doi: 10.1109/ICRA.2017.7989542.

[38] Z. Hu, B. Zhang, and W. Sun, “Cutting characteristics of biological soft tissues,” *CIRP Ann.*, vol. 61, no. 1, pp. 135–138, Jan. 2012, doi: 10.1016/J.CIRP.2012.03.079.

[39] S. Jeong, Y. Chitalia, and J. P. Desai, “Design, Modeling, and Control of a Coaxially Aligned Steerable (COAST) Guidewire Robot,” *IEEE Robot. Autom. Lett.*, vol. 5, no. 3, pp. 4947–4954, Jul. 2020, doi: 10.1109/LRA.2020.3004782.

[40] Z. Zhang, J. Dequidt, J. Back, H. Liu, and C. Duriez, “Motion Control of Cable-Driven Continuum Catheter Robot Through Contacts,” *IEEE Robot. Autom. Lett.*, vol. 4, no. 2, pp. 1852–1859, Apr. 2019, doi: 10.1109/LRA.2019.2898047.

[41] A. Garriga-Casanovas and F. Rodriguez y Baena, “Complete follow-the-leader kinematics using concentric tube robots,” *Int. J. Rob. Res.*, vol. 37, no. 1, pp. 197–222, 2018, doi: 10.1177/0278364917746222.

[42] J. Granna, T. S. Rau, T.-D. Nguyen, T. Lenarz, O. Majdani, and J. Burgner-Kahrs, “Toward automated cochlear implant insertion using tubular manipulators,” in *Medical Imaging 2016: Image-Guided Procedures, Robotic Interventions, and Modeling*, Mar. 2016, vol. 9786, p. 97861F, doi: 10.1117/12.2216854.

[43] K. Oliver-Butler, Z. H. Epps, and D. C. Rucker, “Concentric agonist-antagonist robots for minimally invasive surgeries,” in *Medical Imaging 2017: Image-Guided Procedures, Robotic Interventions, and Modeling*, Mar. 2017, vol. 10135, no. 3, p. 1013511, doi: 10.1117/12.2255549.

[44] C. Girerd, K. Rabenorosoa, P. Rougeot, and P. Renaud, “Towards optical biopsy of olfactory cells using concentric tube robots with follow-the-leader deployment,” *IEEE Int. Conf. Intell. Robot. Syst.*, vol. 2017-September, pp. 5661–5667, Dec. 2017, doi: 10.1109/IROS.2017.8206455.

[45] H. B. Gilbert, J. Neimat, and R. J. Webster, “Concentric Tube Robots as Steerable Needles: Achieving Follow-the-Leader Deployment,” *IEEE Trans. Robot.*, vol. 31, no. 2, pp. 246–258, Apr. 2015, doi: 10.1109/TRO.2015.2394331.

[46] H. S. Yoon, H. J. Cha, J. Chung, and B. J. Yi, “Compact design of a dual master-slave system for maxillary sinus surgery,” *IEEE Int. Conf. Intell. Robot. Syst.*, pp. 5027–5032, 2013, doi: 10.1109/IROS.2013.6697083.

[47] V. Agrawal, W. J. Peine, and B. Yao, “Modeling of transmission characteristics across a cable-conduit system,” *IEEE Trans. Robot.*, vol. 26, no. 5, pp. 914–924, Oct. 2010, doi: 10.1109/TRO.2010.2064014.

[48] G. Palli, G. Borghesan, and C. Melchiorri, “Modeling, identification, and control of tendon-based actuation systems,” *IEEE Trans. Robot.*, vol. 28, no. 2, pp. 277–290, Apr. 2012, doi: 10.1109/TRO.2011.2171610.

[49] S. Lang *et al.*, “A european multicenter study evaluating the flex robotic system in transoral robotic surgery,” *Laryngoscope*, vol. 127, no. 2, pp. 391–395, Feb. 2017, doi: 10.1002/LARY.26358.

[50] H. Choset, A. Wolf, and M. A. Zenati, “Steerable, Follow the Leader Device,” Jun. 24, 2013.

[51] “SOLIDWORKS.” https://www.solidworks.com/ (accessed Dec. 05, 2022).

[52] “K&J Magnetics - Magnet Calculator.” https://www.kjmagnetics.com/calculator.asp?calcType=block (accessed Mar. 17, 2023).

[53] “3D Printing Elephant’s Foot – Easy Fixes | All3DP.” https://all3dp.com/2/elephant-s-foot-3d-printing-problem-easy-fixes/ (accessed Jun. 08, 2022).

[54] “The Wire Used In EDM Machines – The Different Sizes and Types Options.” https://www.camtechedm.com/the-wire-used-in-edm-machines-sizes-and-types/ (accessed Mar. 13, 2023).

[55] V. Zaphiratos *et al.*, “Magnetic interference of cardiac pacemakers from a surgical magnetic drape,” *Anesth. Analg.*, vol. 116, no. 3, pp. 555–559, May 2013, doi: 10.1213/ANE.0B013E31827AB470.

[56] D. Solari, A. Villa, M. De Angelis, F. Esposito, L. M. Cavallo, and P. Cappabianca, “Anatomy and Surgery of the Endoscopic Endonasal Approach to the Skull Base,” *Transl. Med. @ UniSa*, vol. 2, p. 36, Jan. 2012, Accessed: Mar. 29, 2023. [Online]. Available: /pmc/articles/PMC3728777/.

[57] E. Breatnach, G. C. Abbott, and R. G. Fraser, “Dimensions of the normal human trachea,” *AJR. Am. J. Roentgenol.*, vol. 142, no. 5, pp. 903–906, 1984, doi: 10.2214/AJR.142.5.903.

[58] M. Stetter and D. A. Hendrickson, “Laparoscopic surgery in the elephant and rhinoceros,” in *Fowler’s Zoo and Wild Animal Medicine: Current Therapy*, vol. 7, 2011, pp. 524–530.

[59] “Definition of bronchoscopy - NCI Dictionary of Cancer Terms - NCI.” https://www.cancer.gov/publications/dictionaries/cancer-terms/def/bronchoscopy (accessed Mar. 17, 2023).